1-1-2013

High Resistivity Amorphous Selenium Alloy Semiconductors For Radiation Detection Applications

Abhinav Mehta
University of South Carolina

HIGH RESISTIVITY AMORPHOUS SELENIUM ALLOY SEMICONDUCTORS FOR RADIATION DETECTION APPLICATIONS

by

Abhinav Mehta

Bachelor of Technology
Amity University, 2011

Submitted in Partial Fulfillment of the Requirements

For the Degree of Master of Science in

Electrical Engineering

College of Engineering and Computing

University of South Carolina

2013

Accepted by:

Krishna C. Mandal, Director of Thesis

Guoan Wang, Reader

Lacy Ford, Vice Provost and Dean of Graduate Studies

DEDICATION

I would like to dedicate this work to my parents and to my friend for their encouragement and support.

ACKNOWLEDGEMENTS

I am thankful to my advising professor and supervisor, Prof. Krishna C. Mandal, who supported and taught me with great enthusiasm. Under his guidance I have learned new skills and acquired knowledge which will help me throughout my career as an electrical engineer. I would like to thank Prof. Guoan Wang, Electrical Engineering Department, for motivating and supporting my research and also for taking out time to oversee my work as a reader for this thesis.

I would like to express my gratitude to my fellow lab members Dr. Sandeep K. Chaudhuri, Mr. Sandip Das, Dr. Ramesh M. Krishna, Mr. Kelvin M. Zavalla and Mr. Mohamad A. Mannan who have been a source of nonstop guidance and support.

I am thankful to Prof. Arnold Burger and Mr. Michael Groza of Fisk University, Nashville, TN, for characterizing our a-Se alloy materials. I would also like to thank the Electron Microscopy Center of University of South Carolina for SEM studies and EIC Laboratories, Inc. Norwood, MA, USA, for their collaboration.

I would like to thank DOE Office of Nuclear Energy's Nuclear Energy University Programs (Grant No. DE-AC07-05ID14517) for providing partial funding for this research work.

ABSTRACT

High resolution noninvasive tools of diagnosis has always derived and enabled scientific and medical research to probe and better understand subtleties of matter, intangible to the human eye. Radiation detection systems are highly dependent on advancements in materials and devices with front-end electronics. There are various discrete applications of these radiation detectors and each application imposes certain requirements so there is no single optimum radiation detector.

Flat panel x-ray imagers have gained high demand in the past decade because of exponential improvement in readout electronics. We have synthesized and investigated stabilized amorphous selenium (a-Se) alloys suitable for high resolution flat panel x-ray imagers for medical diagnostic applications, primarily in digital mammography and chest radiography systems. Also, in our pursuit to develop high energy physics radiation detectors, we present a novel method to detect neutrons by exploring alpha detection capabilities of isotopic boron doped a-Se alloys.

The synthesis of well-defined a-Se (As, Cl) alloys and boron doped a-Se alloys have been carried out using a specially designed alloying reactor. The alloy composition has been optimized to ensure good charge transport properties and opto-electronic device performance. The synthesis of a-Se (As, Cl) alloys has been carried out by thoroughly mixing zone-refined (ZR) Se (~7N) with previously synthesized Se-As and Se-Cl master alloys. These synthesized alloys were then used as precursor materials for synthesizing isotopically enriched boron doped alloys. To study and verify the desired physical,

electrical, and opto-electronic properties of the synthesized alloys, they have been characterized by various characterization techniques such as scanning electron microscopy (SEM), x-ray diffraction (XRD), glow discharge mass spectroscopy (GDMS), differential scanning calorimetry (DSC), Raman spectroscopy, x-ray photoelectron spectroscopy (XPS), and current-voltage (I-V) characteristics. We have achieved our goal, and have successfully grown stable highly-resistive a-Se alloys and fabricated single layer planar detectors which can perform under high voltage bias with low electronic noise. Results of high energy alpha particle response with a specific signature of thermal neutron detection using boron doped a-Se alloy detector has been successfully investigated and demonstrated.

TABLE OF CONTENTS

LIST OF TABLES

LIST OF FIGURES

CHAPTER 1: INTRODUCTION

1.1 BACKGROUND

High resolution noninvasive tools of diagnosis has always derived and enabled scientific and medical research to probe and better understand subtleties of matter, intangible to the human eye. Radiation detection systems are important for medical, security and research applications.

Currently new materials are being pursued for advancement in detector technology. We need robust semiconductor materials which can offer better resolution, stopping power, detective quantum efficiency and at the same time are compatible with the advancements in electronics.

Amorphous selenium has been an interesting photoconductive material which has proven its use in various radiation detection applications primarily in medical mammography systems. Our interest here at USC is to investigate in-detailed properties after growing, purifying, alloying and characterizing this semiconductor. Our goal is to grow stable high resistivity a-Se alloys and make single layer planar detectors which can perform under high bias with low dark leakage current. Also in our investigation we present a novel method to detect neutrons by exploring alpha detection capabilities of boron doped a-Se alloys. Hence, our studies open a novel avenue of its use as solid-state neutron detectors.

1.2 THESIS OVERVIEW

Amorphous selenium alloy materials were synthesized from purified starting materials to fabricate thin film and bulk alloy devices. Selenium starting materials were purified using the horizontal zone refining (HZR) technique. High quality a-Se-As (9.5%) and a-Se-Cl (50 ppm) master alloys, a-Se (0.52%As, 5 ppm Cl) bulk alloy, and boron-doped a-Se (0.52%As, 5 ppm Cl) bulk alloy were synthesized using a special alloying reactor. The physical, optical, and electrical properties were characterized, and the performances of the fabricated devices were evaluated.

There are six chapters to this thesis. In Chapter 1, evolution of x-ray detectors and a brief introduction to the prevalent techniques and terminologies have been discussed. Also theoretical understanding of flat panel x-ray imagers (FPXI) and a brief survey of the available photoconductors are also provided.

Chapter 2 describes the zone purification method used to purify starting Se precursor material. The efficacy of zone-purification was measured by impurity analysis of the zone-refined Se samples using glow discharge mass spectroscopy (GDMS) techniques. The chapter also elaborates on techniques used to synthesize good quality a-Se (As), a-Se (Cl) master (MS) alloys, a-Se (As, Cl) bulk alloys, and finally, boron-doped a-Se (As, Cl) bulk alloys. The results of composition analysis by mass-spectroscopy for different alloy materials are also discussed here. Finally, the fabrication process of the a-Se (As, Cl) alloy films on ITO/Al substrates are described in this chapter.

Chapter 3 describes various characterization techniques used to analyze physical, electrical, optical, and spectroscopic properties of the synthesized a-Se alloys and alloy films. Results of characterization techniques such as scanning electron microscopy

(SEM), x-ray diffraction (XRD), differential scanning calorimetry (DSC), Raman spectroscopy, x-ray photoelectron spectroscopy (XPS), and current-voltage (I-V) characteristics are explained here.

Chapter 4 describes the fabrication and characterization of heavily B-doped a-Se (As, Cl) alloy films for its use as thermal neutron detector. Current-Voltage characteristics of the boron doped alloy films are then obtained at different temperatures, resistivity is determined, and photosensitivity is recorded.

Chapter 5 describes the step involved in fabrication of single layer planar detectors based on B-doped a-Se alloys and device characterization with high energy alpha particles to demonstrate the device application for neutron detection.

Finally, Chapter 6 concludes our work and discusses avenues for future research.

1.3 Background of X-ray Detectors

X-ray detectors or imagers were first developed for medical applications, which at that time was the primary source for its investigation [1]. At the time of its discovery, Crookes tube was the source of x-rays and soon radiographic films were developed to detect them. This detection scheme consisted of a scintillator (phosphor screen) which is used to convert incoming x-ray photons to optical photons. These photons, which contain the required information, are then recorded by photographic film emulsions and consequently an analog image is created after chemical processing. This screen film (SF) technique has been optimized, over the years, for acceptable stopping power and spatial resolution. However, this technique suffers from different limitations; the image has to be acquired via chemical exposure and the information is stored in a fragile analog form, so it cannot be remotely accessed, shared or transferred. Also the duplicate image is of lower

quality, requires cumbersome work and incurs more cost. For better image quality a higher radiation exposure is required, which poses a threat to human health.

Hence for the past 40 years, research has been geared towards digital x-ray imagers. Digital radiography allows the use of advanced imaging techniques over screen film technology. This technique has slowly evolved to give high detection efficiency, and better spatial, temporal, and energy resolution [1]. Also detection can be performed at lower radiation exposure, which is of key interest in medical applications. Images with better quality and display contrast are readily available for remote access and consultation. The digital x-ray detectors are primarily divided into two broad categories, storage-phosphor radiography (SPR) and digital radiography (DR) systems [2].

Radiation detectors based on SPR technique were made commercially available in the early 1980's and primarily consists a phosphor system that captured the incident x-rays as a latent image, which is a distribution of electronic charges trapped in a metastable energy level in the phosphor. This latent image formed by the electrons is developed by illuminating the phosphor with red or near infrared laser. This expose and read process involves a mechanical scanning step (scanning of the phosphor plate) and hence results in poor efficiency and quality primarily because of noise [2].

Digital radiography (DR) has characteristic electrical readout capabilities and is subdivided into two techniques. Firstly, there are indirect conversion detectors in which the x-rays scintillating phosphors such as CsI(Tl), Gd_2O_2S(Tb) convert the incoming x-rays to light. This light is then detected by a secondary quantum detector or a digital flat panel x-ray image detector which is usually comprised of an array of photodiodes, thin film transistors (TFT), complementary metal oxide semiconductors (CMOS) or charged

coupled devices (CCD) [2, 3]. These indirect conversion detectors have high detective quantum efficiency (DQE) at higher frequencies but have poor resolution because of light diffusion inside the scintillator. Secondly, there are direct conversion detectors which are more efficient as they use a photoconductor (primarily a-Se) to absorb the incident x-ray photons and directly convert them into charge carriers (electrons and holes) which are collected by an appropriately designed active matrix array (AMA). There are various discrete applications of these radiation detectors and each application will impose certain requirements so there is no single optimum radiation detector. Several photoconductors have been explored and investigated as x-ray detectors for large area applications. Properties, such as, attenuation depth (δ), bandgap energy (E_g), electron-hole pair generation energy (W), and carrier range (mu-tau products) of electrons and holes, for some of these photoconductors for x-ray detector are compared in Table 1.1.

Practical constraint such as large area fabrication, charge collection efficiency, x-ray sensitivity, detective quantum efficiency (DQE) and unacceptable dark current (leakage current) limits potentially good photoconductors such as TlBr [4, 5], PbI_2 [6, 7], HgI_2 [6, 7, 8, 9], CdZnTe [10, 11, 12, 13, 14] and PBO [15, 16]. Currently, only a-Se based FPXIs have been commercialized and are popular for their high quality mammography images [17].

Table 1.1. Properties of prevalent x-ray detectors for large area applications.

Photoconductor State Preparation	**δ at 20 keV δ at 60 keV**	E_q **eV**	$W_{\pm}$ **eV**	**Electron** $\mu_e\tau_e$ **(cm²/V)**	**Hole** $\mu_h\tau_h$ **(cm²/V)**
Stabilized a-Se Amorphous Vacuum deposition	49 μm 998 μm	2.2	45 at 10 V/μm 20 at 30 V/μm	$3\times10^{-7} - 10^{-5}$	$10^{-6} - 6\times10^{-5}$
HgI_2 Polycrystalline PVD	32 μm 252 μm	2.1	5	$10^{-5} - 10^{-3}$	$10^{-6} - 10^{-5}$
HgI_2 Polycrystalline SP	32 μm 252 μm	2.1	5	$10^{-6} - 10^{-5}$	$\sim10^{-7}$
$Cd_{.95}Zn_{.05}Te$ Polycrystalline Vacuum deposition (sublimination)	80 μm 250 μm	1.7	5	$\sim2\times10^{-4}$	$\sim3\times10^{-6}$
PbI_2, Polycrystalline Normally PVD	28 μm 259 μm	2.3	5	7×10^{-8}	$\sim2\times10^{-6}$
PbO, Polycrystalline Vacuum deposition	12 μm 218 μm	1.9	8 – 20	5×10^{-7}	small
TlBr Polycrystalline Vacuum deposition	18 μm 317 μm	2.7	6.5	small	$1.5 - 3\times10^{-6}$

1.4 Introduction to FPXIs Based on Amorphous Selenium

In 1959 Xerox used amorphous selenium based copiers to revolutionize document reproduction since then there has been a growing interest in understanding the xerography and xeroradiography properties of this excellent photoconductor [18]. Even though a-Se has been replaced by inexpensive organic photoconductors its use in xeroradiography is still prevalent [19]. Over the years various readout techniques helped

in the modernization and development of these detectors but they have all revolved around the same basic principle. The a-Se photoconductor surface is charged positively i.e. an appropriate bias is applied and then it is exposed to the incident x-rays which selectively photo-discharged its surface passing via the scanned object of interest. Various read out techniques have been incorporated as the secondary quantum detectors for this charge distribution [20, 21]. Even though a-Se can be deposited over large areas but the small area of the readout electronics limited what could be achieved. Recent development in the a-Si:H (hydrogenated amorphous silicon) based AMAs has revolutionized and modernized these detectors in the form of flat panel x-ray imager (FPXI). FPXIs are being widely used and gaining popularity in various x-ray imaging applications. This can be primarily attributed to the fact that x-rays cannot be focused and this limitation necessitates that the detectors have a large area. An AMA is a two dimensional array of pixels in which each pixel has a TFT (based on a-Si:H) and a storage capacitor. The AMA is coated by a-Se and appropriate bias of about 10V/µm is applied across the surface [17]. Now after the application of the bias an electric field is established inside the photoconductor which allows the electron hole pairs (EPHs) to drift across the a-Se absorber layer and eventually get collected by the respective pixels. These collected charges on the array of pixels are then according addressed and read which forms final signal (digital image) [22, 23]. The schematic of operation is depicted in Figure 1.1. The gate of the TFTs is connected to the address line and when a read signal is applied it allows conduction of charge through the storage capacitors. This charge then flows to a data line, output amplifier, analog to digital (A/D) converter and then finally as a pixel of the hence formed image [17].

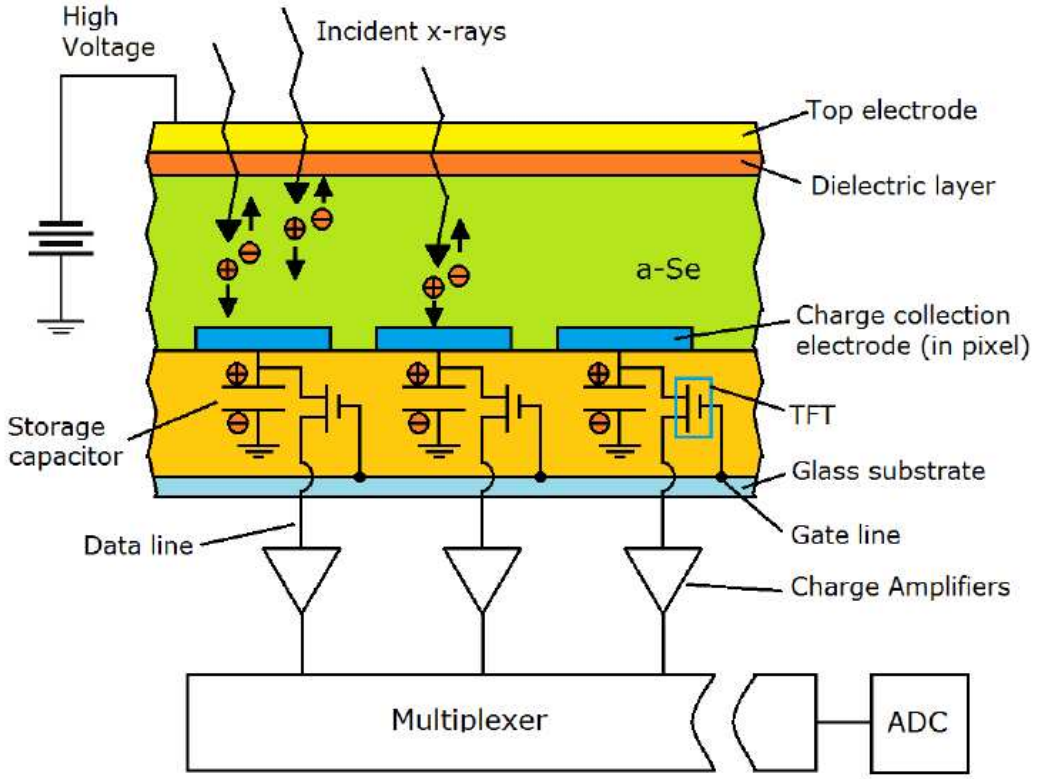

Figure 1.1. Schematic diagram of read-out in a-Se based FPXIs.

1.5 MATERIAL AND ELECTRICAL PROPERTIES OF AMORPHOUS SELENIUM

In practical development resolution is compromised in some aspects and optimized in certain aspects. Even though the recent development in the electronics of these detectors lead to their exponential development, these detectors are still lagging behind the excellent sources that have already been developed. The focus in the detector research is towards more robust materials which can be coated uniformly with the required thickness over large areas (such as 24 cm × 30 cm for mammography) and at the same time have better detection and x-ray stopping capabilities [24]. Ideally a semiconductor must have the following properties:-

- X-ray Photoconductivity: An ideal photoconductor will have high x-ray sensitivity. Ionization energy or electron-hole pair generation energy ($W_{\pm}$) is defined as the amount of radiation energy required to generate a single free electron-hole pair in the semiconductor. Usually semiconductors with narrow band-gap have high x-ray sensitivity and the follow Klien rule i.e. $W_{\pm} = 3E_g$. Thus it is intuitive to conclude that $W_{\pm}$ should be as low as possible but more importantly this generated charge has to be efficiently collected. Many polycrystalline semiconductors have lower $W_{\pm}$ as compared to a-Se but currently lack the good charge collection efficiency [25].
- Low Dark Current: When a high bias is applied to photoconductor it leads to the generation of dark current. This current is typically from the thermal generation of carriers and/or injection of carriers from the biased contacts at high fields. This is called dark current because it is independent of the incoming photons. Semiconductors with wide band gaps have low thermal generation but have low photoconductivity. Blocking contacts are deposited to retard the injection of carriers but they have to be optimized so that they allow the charges generated by x-rays to exit the photoconductor, which will constitute the signal. Currently commercially available a-Se FPXIs solve this problem by depositing electron and hole blocking layers to the respective contacts. Our goal here at USC is to grow high resistivity a-Se alloys and make single-layer direct-readout planar detectors which can perform under high bias with low dark current.
- Charge Collection: When electron-hole pairs (EPHs) are generated by the incident x-rays they drift towards respective electrodes under the influence of the applied bias but some of the carriers are lost due to recombination and traps in the photoconductor. The EHPs should be able to travel farther and reach the electrodes. “Schubweg” is defined as

the mean distance traveled by a carrier in a field before it is trapped and it is given by the product of μτE [21], where:-

— μ is the drift mobility

— τ is the lifetime

— E is the applied field

Hence "μτE" for both electrons and holes should be greater than the detector thickness (L). In case of polycrystalline semiconductors carrier range (μτ) greatly depends on the purity and is affected by crystal defects. Whereas carefully alloyed a-Se (stabilized with As and Cl) has good charge collection efficiency for both electrons and holes [21, 26].

- Quantum Efficiency (A_Q): The x-rays should be absorbed in the material and this property is controlled by the absorption coefficient "α", which depends on the energy of the incident x-rays and also on the atomic number "Z" and density "ρ" of the material. Ideally "Z" and "ρ" should be as high as possible. It is also of prime importance that the radiation is absorbed within the detector, limiting radiation exposure to patients. Photoconductor thickness "L" should be greater than attenuation depth "δ" or "1/ α". From Figure 1.2 we can see that at around 20 keV a 200 μm a-Se the attenuation depth is 49 μm which corresponds to 98.3% A_Q which is the case with commercially available mammography systems. Also other photoconductors with high "Z" such as PbO, HgI_2 which have better quantum efficiencies, should be considered for general radiography purposes.

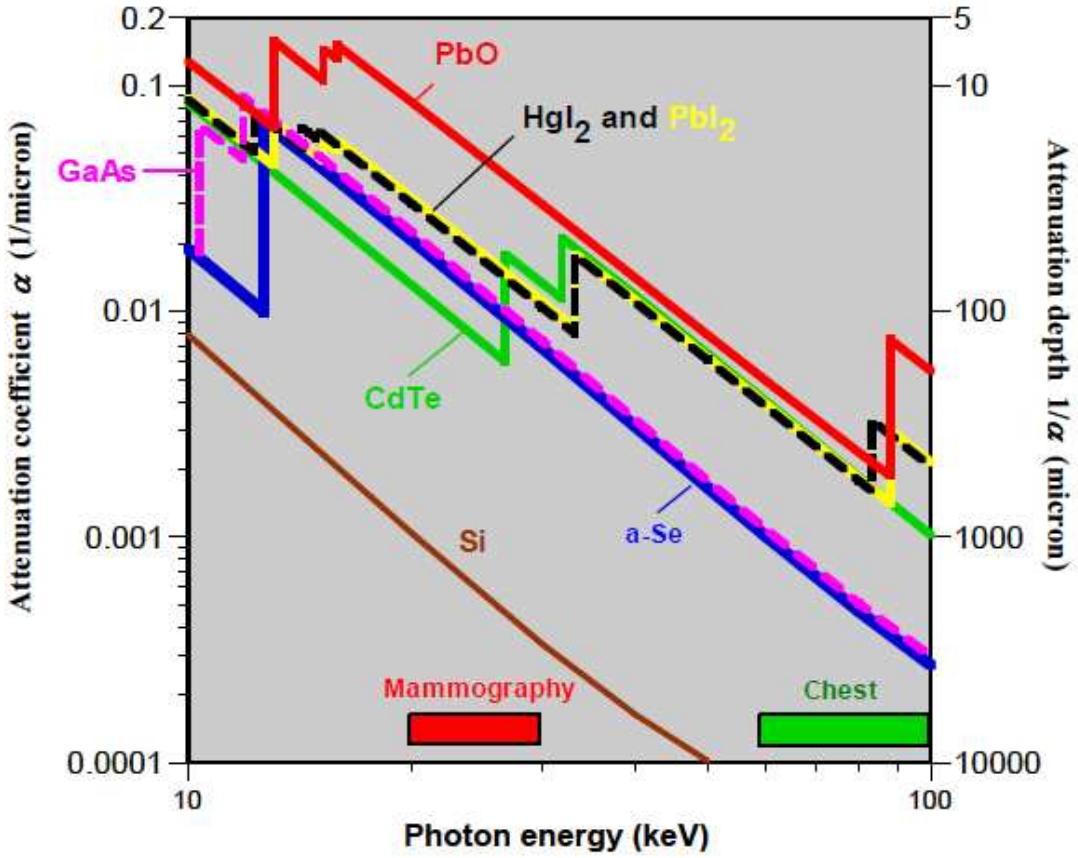

Figure 1.2. Linear attenuation coefficient "α" and depth "δ" or "1/ α" to photon energy for respective photoconductors.

Crystalline semiconductors are difficult to grow in large areas and their process temperature (typically 900°C) is incompatible with the glass AMA substrate and its a-Si:H electronics. As a-Se is a highly developed photoconductors, thanks to its history of use in xerography, conventional technique of vacuum deposition can be used to deposit thick a-Se layers (1200 µm) over large areas. Substrate temperature of 60-70°C is required for deposition of amorphous films, which is compatible with a-Si:H TFT-AMA substrates. Now as this film is amorphous it can be optimized with uniform

characteristics over large areas. Some prevalent physical properties of a-Se are listed in Table 1.2.

Table 1.2. Physical properties of a-Se.

Physical Properties	**a-Se**
Atomic Weight	78.96
Atomic Number	34
Covalent Radius	1.16 A
Ionic Radius	1.98
Electronegativity	2.55
Electronic Structure	[Ar] $3d^{10}$ $4s^2$ $4p^4$
Density	4.29 (gm^{-3})
Glass transformation temperature (T_g)	48-50°C
Crystallization temperature (T_c)	100-102°C
Melting Temperature	218°C
Micro-hardness (Vickers hardness number)	40 (kgf/mm^2)

1.6 ALLOYING CONSIDERATIONS FOR STABILIZED AMORPHOUS SELENIUM

It can be observed from Table 1.1 that the hole range is almost an order of magnitude greater than that for electrons, and this is because a-Se is p type like all other chalcogenide glasses. Mostly, chalcogenide are unaffected by the addition of impurities as compared to crystalline semiconductors but a-Se is very sensitive to the addition of certain impurities and this behavior can be tuned to our advantage.

Pure amorphous selenium tends to crystallize over time, resulting in a sharp reduction of resistivity and hence leads to undesirable high dark current. When arsenic (As) is alloyed with a-Se, arsenic triply bonds with selenium making cross-links between Se-chains (Figure 1.3) [27]. This increases viscosity retarding crystallization.

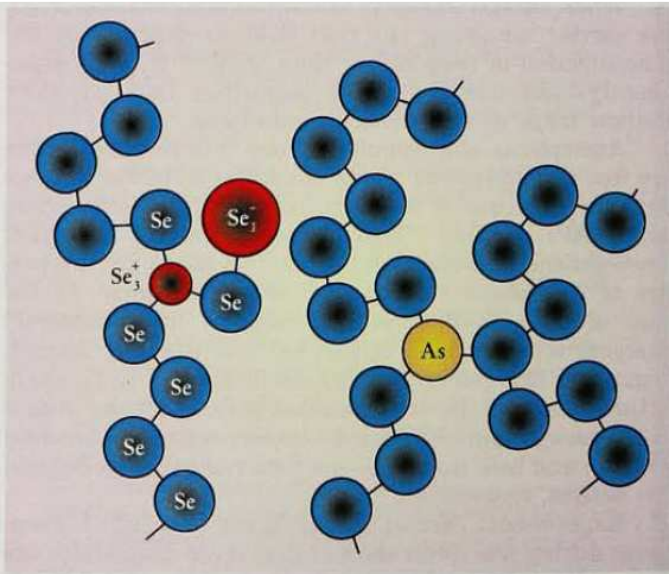

Figure 1.3. Structure of a-Se depicting Se chains valence alternation pair defects and triply bonded As in the Se chain.

There are various tradeoffs with arsenic addition as it decreases hole transport by decreasing hole lifetime, it reduces electron mobility but increases electron lifetime

resulting in a net increase in electron transport. In order to improve hole transport chlorine (Cl) is added in the parts-per-million (ppm) range which counteracts this effect but negatively affects electron transport [28]. The effects on the electronics properties of a-Se due to arsenic and chlorine doping are summarized in Figure 1.4. Consequently, it has been found that arsenic and chlorine doping stabilizes the amorphous structure and significantly improves the electrical properties of a-Se as shown in Table 1.3 [29]. However, a careful control of alloying parameters is crucial [30].

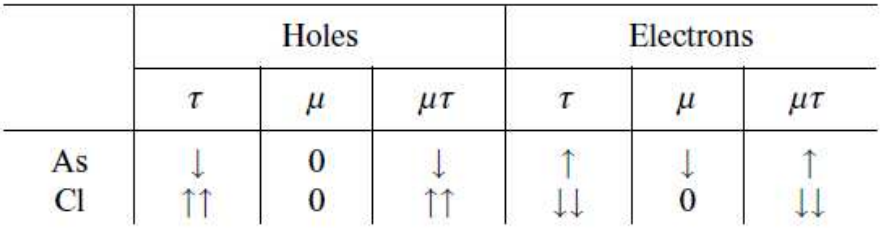

Figure 1.4. Effect of Arsenic and Chlorine on the electronics properties of a-Se.

Table 1.3. Electrical properties of a-Se and stabilized a-Se alloyed with arsenic and chlorine as found in literature.

	a-Se Alloy (0.3%As +5ppm Cl)		a-Se	
	Electrons	Holes	Electrons	Holes
Lifetime, τ (μs)	342	77.6	155	10.2
Mobility, μ ($cm^2V^{-1}s^{-1}$)	2.86×10^{-3}	0.1183	4.107×10^{-3}	0.129
Charge-carrier ranges, μτ (cm^2V^{-1})	9.79×10^{-7}	9.18×10^{-6}	6.37×10^{-7}	1.32×10^{-6}
Bandgap energy, E_g (eV) at 300 K	2.2		1.74	
Work Function, χ (eV)	5.88		5.88	

1.7 INTRODUCTION TO BORON DOPED AMORPHOUS SELENIUM ALLOYS

Thermal neutrons are among the most useful probes for investigation of the structural, magnetic and acoustic properties of materials. As a sustainable energy source, nuclear energy has become an important component of nations' energy portfolio. With domestic and global expansion of nuclear power and development of nuclear fuel cycle processes, there are growing concerns about the nuclear proliferation and nuclear terrorism risk arising from potential access to special nuclear materials (SNMs) enrichment and reprocessing technologies. Thus deployment of portable, high performance, solid-state nuclear spectrometers are needed for international safeguards to monitor used fuel recycling activities, verification of nuclear non-proliferation treaty, and surveillance of nuclear terrorism activities. The demands of such detector are not fully covered by the current detection system

Current methods of thermal neutron detection by large cumbersome gas proportional counters or scintillator-photomultiplier tube combinations are limited by their detection efficiency, stability of response, speed of operation, and physical size. [31, 32, 33, 34] Furthermore, world-wide shortage of ^{3}He gas has further prompted to design an alternative system. Therefore, a solid-state neutron detection system without the requirement of ^{3}He will be highly desirable. To address these needs, our research group at USC is carrying out research to construct a large-area, lightweight, high-resolution, and very fast position sensitive thermal neutron detector based on a highly boron-doped amorphous selenium alloy film.

The proposed material has been identified for its many favorable characteristics - a wide bandgap (2.22 eV at 300 K) for room temperature operation, high glass transition

temperature (tg ~84.6°C), a high thermal neutron cross-section (3840 barns, 1 barn = 10-24 cm^2), low effective atomic number of Se for small gamma ray sensitivity, and high radiation tolerance due to its amorphous structure. Very large area neutron detectors (≥square meters) can be fabricated by tiling individual detectors using an already established technology from medical imaging field [35].

In pursuit of a neutron detector natural isotropic boron (^{10}B) doped a-Se (As, Cl) alloy materials were prepared. The use of boron-doped a-Se (As, Cl) film as an efficient thermal neutron detector relies on the presence of ^{10}B, which has a natural isotopic abundance of 19.9%, but is also available in an enriched form (≥95%). The ^{10}B nucleus has a large cross section for thermal neutrons (3840 barns), and the neutrons when captured by the ^{10}B nucleus undergo an (n, α) reaction, producing two energetic charged particles [33, 34].

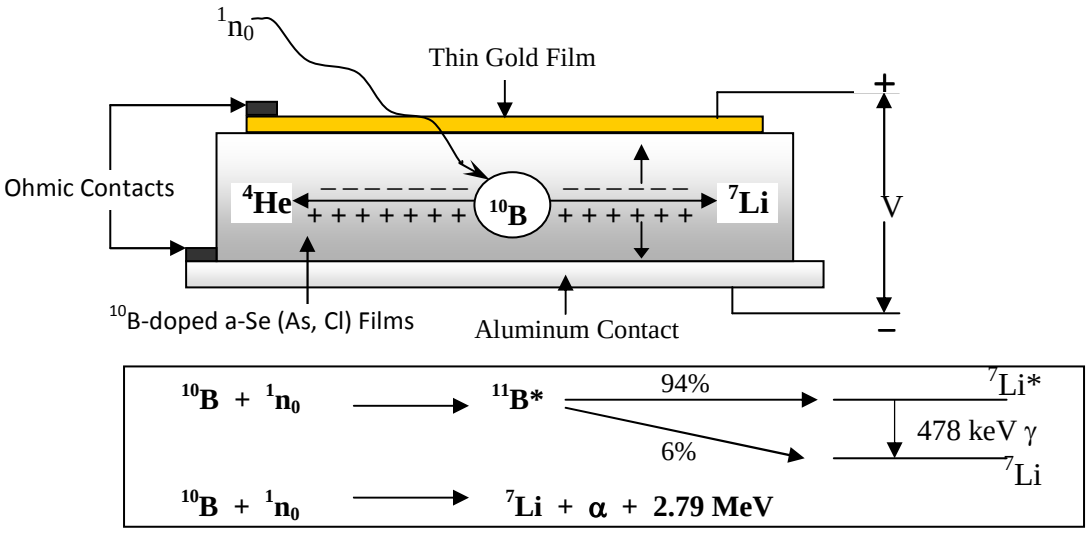

Figure 1.5. Conceptual design of a thermal neutron detector using B-doped a-Se (As, Cl) semiconductor films

The released 2.79 MeV kinetic energy is shared by the two charged particles traveling in opposite directions (energy of ^{7}Li = 1.014 MeV and E_{α} = 1.78 MeV). As with any charged particles of this energy, they have relatively short path lengths in solid materials and would be readily stopped, depositing their kinetic energy. The kinetic energy of the charged particles excites electrons into the lattice conduction band and displaces atoms from their lattice sites. The general rule-of-thumb for energetic light ions in semiconductors is that for every two to three times the bandgap in energy deposited, one electron hole pair is created. The electrons excited into the conduction band (and holes in the valence band) are free to move and can produce a measurable electrical current upon application of an electric field across the a-Se film. The resulting signal pulse indicates the occurrence of a thermal neutron capture event. Standard nuclear-pulse type, charge-sensitive amplifier electronics are used to measure the current pulses.

Since boron doped a-Se (As, Cl) alloys directly produce alpha particles upon neutron irradiation, the detector is capable to monitor alpha events. Hence, if we can monitor the alpha particle response, we can indirectly account for neutrons. In chapter 5 we show preliminary studies that validates charged particle response using alpha particles as a surrogate for neutrons. This minimizes the need for use of expensive neutron beam time and/or the radiologically more challenging neutron source at this initial phase of testing. A collimated alpha beam is employed to measure the uniformity of detector response across a larger detector.

CHAPTER 2: PREPARATION OF AMORPHOUS SELENIUM

2.1 OVERVIEW

Commercially available selenium (Se) typically has a purity of 5N (99.999%). Amorphous selenium (a-Se), as discussed previously, is sensitive to the addition/presence of impurities even in the ppm range. We know a-Se based detectors are operated under high fields like 10V/μm. Now if impurities are present in the a-Se alloy they can create native point defects, which may act as trapping or recombination centers which limit carrier collection. Also their presence can lead to charge buildup and influence the uniformity of the electric field. This non-uniform distribution of electric field will produce a non-uniform electrical response across the detector which can seriously limit the device performance.

Therefore commercially available selenium was further purified using an in-house horizontal multi-pass zone refining (ZR) system. Also in our efforts to make stabilized a-Se alloys with desired electrical properties we have devised a custom deposition setup and installed. The procedure primarily involves mixing of the in-house zone-purified Se with respective impurities with desired composition in an alloying reactor shown in Figure 2.6. This unique alloying reactor was used to synthesize master and bulk alloys of a-Se with different compositions.

2.2 PURIFICATION OF SELENIUM PRECURSOR MATERIAL

2.2.1 Zone Refining Technique

Zone refining (ZR) was developed as a method of purifying various semiconductor materials in the 1950's. [36] This refining method is based on the fact that most impurities distribute differently in solid and liquid phases at equilibrium. If a section of solid material is melted (a 'zone') and we maintain the molten zone while slowly passing through the feed material, in a continuous fashion, this will result in the re-distribution of impurities in the remaining solid. If this process is repeated many times (multi-pass zone refining) the resulting solid would become extremely pure at one end Figure 2.1. In general, the solubility of impurities is larger in the liquid than in the solid phase. Hence, impurities are transported with the molten zone and relatively pure material is left behind.

The extent of zone refining purification depends on the impurity segregation constant, $k = C_S/C_L$, between the solid and liquid states. At thermodynamic equilibrium, C_S is the impurity concentration in the solid phase and C_L is the impurity concentration in the liquid phase. Hence at small k value, one can expect effective zone-purification because now impurities have an increased preference to stay in the melt as shown in Figure 2.2. As we repeat the process (a multi-pass zone refining process) will enable us to obtain extremely high purity precursor materials as shown in the theoretical computations in Figure 2.3.

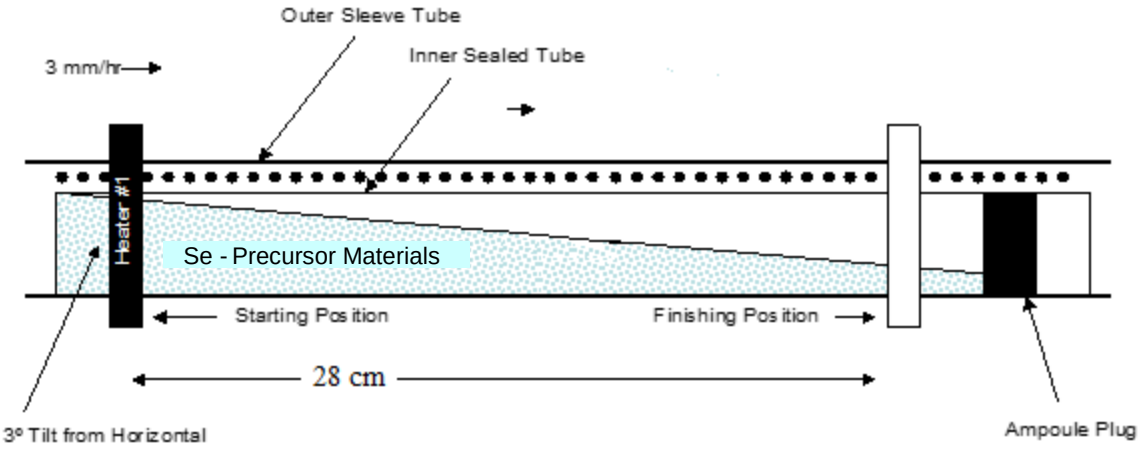

Top down view of single molten zone

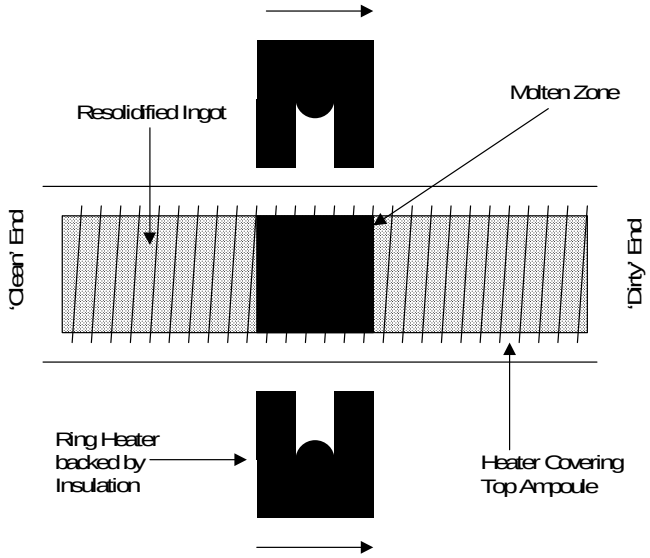

Figure 2.1. A schematic of the zone refiner used to purify Se precursor materials. The heater ring slowly traverse the length of a sealed ampoule containing the Se precursor material to be zone refined. The heater ring melts Se material, each creating a 1" molten zone that moves through the feed material from one end to the other end (left to right). As the liquid Se re-solidifies, it becomes more pure, while the impurity moves with the molten zone.

.

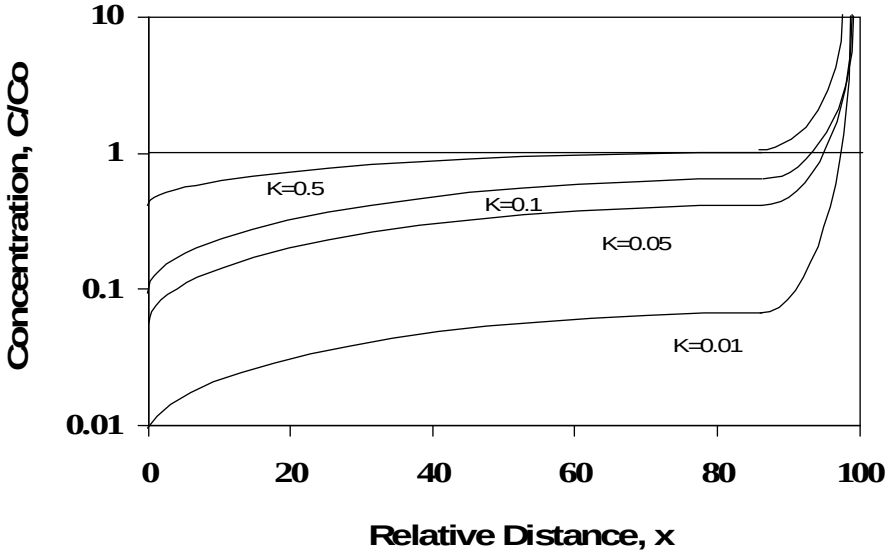

Figure 2.2. Numerical calculations of specific impurity concentration (C/C_0) vs. relative distance along the axial direction of the feed material for various distribution constants k = C_s/C_l with a single scan. Interfacial thermodynamic equilibrium has been assumed for this computation.

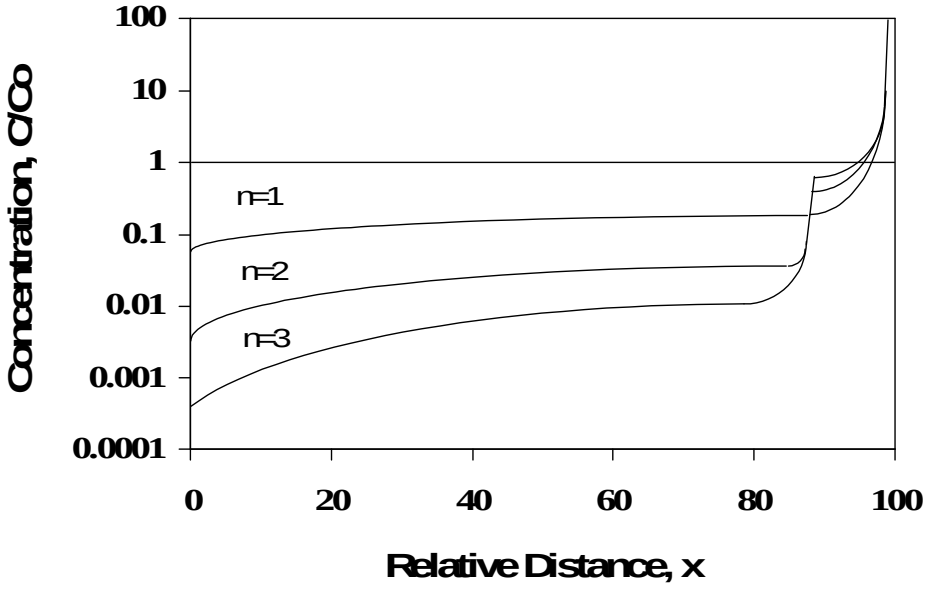

Figure 2.3. Numerical calculations of relative impurity concentrations (C/C_0) vs. distance along the axial direction of the feed material for a hypothetical liquid zone refining process with distribution constant k = 0.05, n is the number of scans (passes).

2.2.2 Ampoule Preparation for Zone Refining

The preparation for the zone refining process involved cleaning the ampoule, filling it with the selenium material (shot form), removing water and other volatile contaminants by heating under a vacuum, and finally sealing the ampoule.

The quartz ampoule used for the zone refining process were manufactured by Quartz Scientific, Inc. (length = 50 cm, OD = 19 mm and ID = 16 mm). The first 30 cm was used to hold the Se and the remaining 20 cm was used as a 'handle' once the ampoule was sealed. The open ampoule was then thoroughly cleaned using the following successive cleaning process:

- ✓ Soak with acetone one time for 5 minutes.
- ✓ Soak with methanol one time for 5 minutes.
- ✓ Etch with 10% HF (aqueous) for 5 to 10 minutes.
- ✓ Rinse with de-ionized water (18 MΩ) at least 10 times and then dry with argon gas.
- ✓ Bake the clean ampoule overnight at 750^{o}C under argon flow (~0.25 liter/min).

The precursor Se shots with a stated purity of 5N were purchased from Alpha Aesar for the zone refining process. It was purchased in 500-g lots, which were convenient to the capacity of the zone refiner. Because the Se shots packed rather loosely in the ampoule, the feed material was melted first into a continuous solid mass by using a separate resistance heated tube furnace. The Se feed material was then loaded into the cleaned, open ampoule. A quartz plug was inserted approximately 12 inches above the bottom of the ampoule. The ampoule was then evacuated to $2x10^{-6}$ Torr while simultaneously being heated to about 150^{o}C to remove any water vapor or volatile organic contaminants from the feed material. After reaching a $2x10^{-6}$ Torr vacuum, a

hydrogen-oxygen torch was used to seal the tube in preparation for the ampoule being loaded into a horizontal tube casting furnace.

A casting step melted the shot form of Se into a long polycrystalline ingot suitable for horizontal zone refining. The recrystallized ingot stayed at the bottom half of the ampoule and stretched almost the full 12" length. This required a furnace temperature of about 275-290^{o}C (melting point of Se is 221^{o}C) for 2 hours.

Next the zone refining process, which involved many passes and took several days, segregated impurities from one end of the bulk material to the other end. The ZR process for Se was conducted in a specifically designed horizontal zone refiner equipped with a single-zone furnace. One of the principal reasons for using horizontal zone refining was to provide room for expansion of the Se material upon melting and thereby eliminate the problem of cracking ampoules. The solid Se-ingot reached only half the radial width of the ampoule. Hence the material had enough room to expand without creating stresses in the quartz.

The heater ring temperature was maintained at 255°C using a temperature controller. When the heater rings reached steady state at the regulated set temperature, the computer was programmed to execute the zone refining route. A preset program controlled the motion of the heater. The heaters were moved very slowly (4 cm/hr) across the length of the ampoule until they passed the entire ampoule. At this stage, the direction of motion was reversed and the heaters returned to the starting point rapidly. The fast pace ensured that none of the ingot melts during the reverse motion. This constitutes one zone refining pass.

After a number of zone refining passes, the effect of purification is even evident to the naked eye. The material in the starting region looked shiny and pure, while the material at the end region (where impurities were segregated) looked dark and dull. After completing 27-45 passes, the purest part of the Se-ingot was removed, typically done in an argon-controlled glove-box environment. The ampoule was cut open by scribing and snapping, and the material was removed from the ampoule. For each ZR run, the impure end of the Se-ingot was cropped from the pure material by breaking the ingot material mechanically. The amount of ingot material determined as 'cleaned' was chosen by uniformity of shiny color. The removed ingots were then stored separately in argon-filled polyethylene bottles; each was labeled to keep track of the starting Se-material and ZR run number. The appearance of the zone refined Se ingots is shown in Figure 2.4.

Figure 2.4. Zone refined a-Se ampoule after 27 cycles.

2.2.3 Impurity Analysis of Zone Refined Selenium

To examine the outcome of ZR process, zone-refined selenium material were analyzed using glow discharge mass spectrometry (GDMS) to determine the presence and concentration of different impurities and compared to that of non-ZR Se samples. Samples were tested for 72 elements from Li to Pb. A typical GDMS analysis data are

presented in Table 2.1, which shows concentrations of elemental impurities in Se material before and after zone refining. The data clearly demonstrate that the impurities were segregated at 'the impure end' of the zone refined material, and the impurity concentrations in Se material were reduced up to 400% by ZR process after 27 passes. The impurity concentrations were further reduced after 40 ZR passes as shown in Table 2.2. The results confirmed that purification by ZR process reduced several dopant impurities in commercially bought Se precursor. This 'zone-purified' Se material was then used to make Se-alloys.

Table 2.1. A typical impurity analysis data by GDMS.

Impurity Elements	Concentration, ppmw		Impurity Elements	Concentration, ppmw	
	Impure End	Pure End		Impure End	Pure End
Se	Major	Major	Mn	0.10	0.01
Li	<0.05	<0.05	Fe	0.30	0.06
Be	<0.05	<0.05	Co	<0.01	<0.01
B	0.05	0.03	Ni	0.05	0.02
Na	0.95	0.22	Cu	0.20	<0.1
Mg	0.10	0.06	Zn	<0.1	<0.1
Al	0.22	0.10	Zr	<0.1	<0.1
Si	7.6	1.5	Mo	<0.1	<0.1
P	0.11	0.045	Ag	≤1	≤1
S	1.0	<0.5	Sn	<0.5	<0.5
Cl	0.80	0.18	Sb	0.13	≤0.1
K	0.20	0.08	Te	<0.5	<0.5
Ca	0.50	0.1	Hf	<0.1	<0.1
Ti	0.022	≤0.01	W	<0.1	<0.1
V	<0.01	<0.01	Hg	7.5	<1
Cr	0.15	0.1	Pb	0.25	0.10

Table 2.2. Impurity analysis by GDMS showing reduction in elemental impurity (dopant) concentration in Se material after zone-purification.

Element	Concentration before ZR	Concentration after ZR
Se	Major	Major
Hg	6-8 ppm	<4 ppb
Pb	16 ppm	<6 ppb
Sn	12 ppb	Not Detected
Ag	4-6 ppm	Not Detected
Cu	25 ppm	0.2 ppm
Fe	10 ppm	Not Detected
Mg	6 ppm	Not Detected
Si	4-6 ppm	0.4 ppm
Te	6-8 ppm	0.35 ppm
H_2O	10-12 ppm	Not Detected

2.3 AMORPHOUS Se (As, Cl) ALLOY SYNTHESIS

2.3.1 Introduction to Alloying Reactor

The preparation of well-defined and high quality a-Se (As, Cl) alloy material was conducted using a specially designed alloying reactor, which is schematically presented in Figure 2.5. After zone purification, the respective alloy ingredients are measured and mixed in the reactor. A picture of the alloying reactor is shown in Figure 2.6. The reactor operation is customized with a specific temperature profile for each alloy. The Process cycle was operated in a glove box maintained in a pure argon atmosphere.

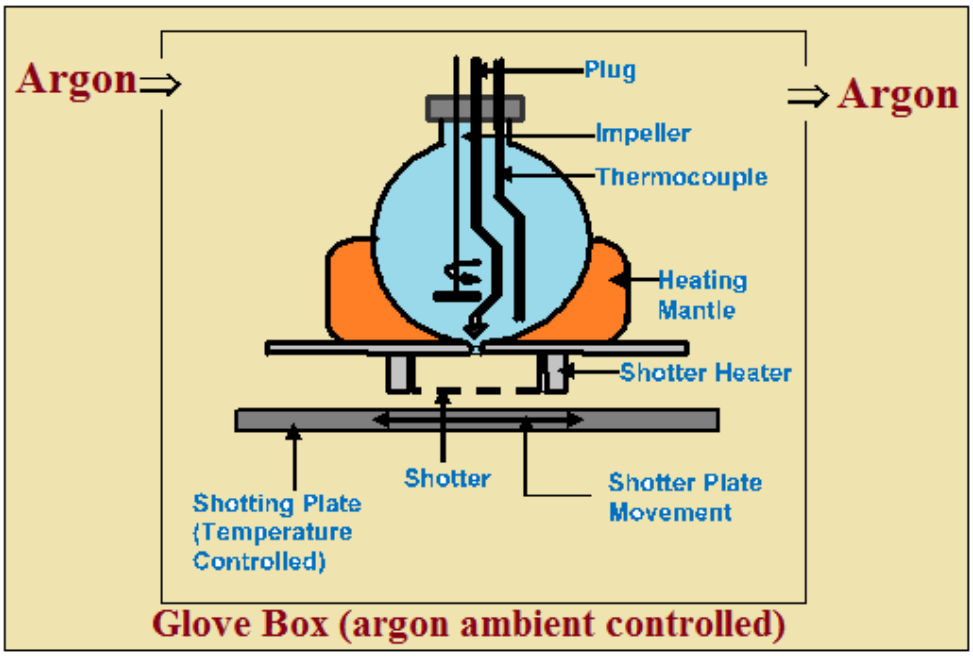

Figure 2.5. Schematic diagram of a-Se alloying reactor.

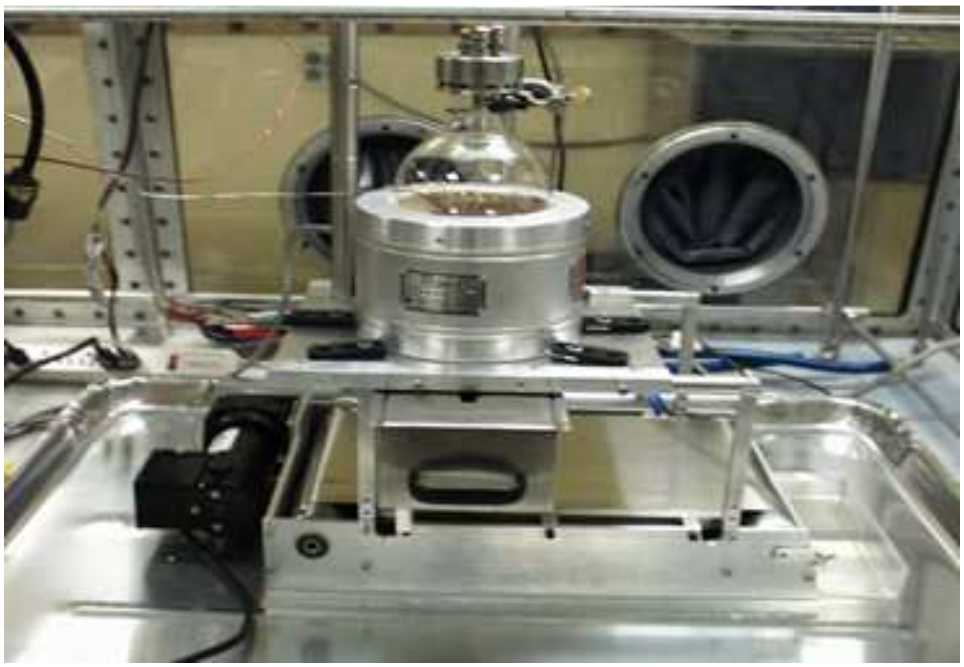

Figure 2.6. Picture of an alloying reactor setup.

2.3.2 Master alloy synthesis

To prevent/retard crystallization rate of amorphous selenium, it was alloyed first with As. During our effort to make a-Se (As, Cl) alloys, we have found that a-Se with an As content of ~0.52% is totally resistant to crystallization. It has also been reported to improve the mobility-lifetime product for electrons and to reduce that of holes. A very small amount of Cl (~5 ppm) compensates the effect of As on the charge transport characteristics and drastically increases the lifetime of holes, while it decreases that of electrons [37].

In order to prepare a-Se (As, Cl) alloys, first adequate quantities of selenium arsenic master alloys (Se-As) and selenium chlorine master alloys (Se-Cl) were synthesized. For Se-As master alloys, zone refined selenium was crushed and mixed with 99.9999% pure commercially available arsenic. Similarly Se-Cl master alloy was made by mixing zone refined selenium and $SeCl_2$. The flow sheet diagrams, the temperature profiles of master alloy (Se-As and Se-Cl) synthesis and the pictures of alloy shots are presented below in Figures 2.7 to 2.12.

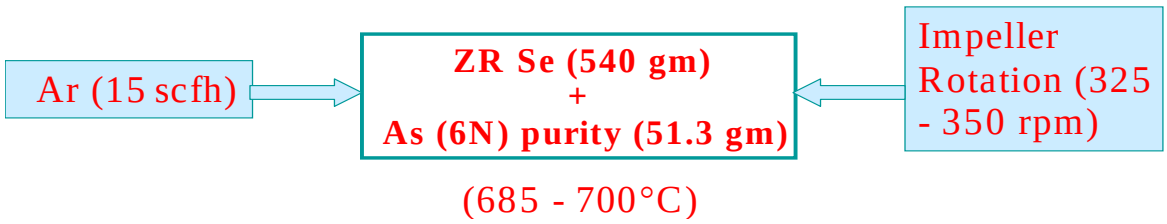

Figure 2.7. Synthesis of Se-As MS alloy.

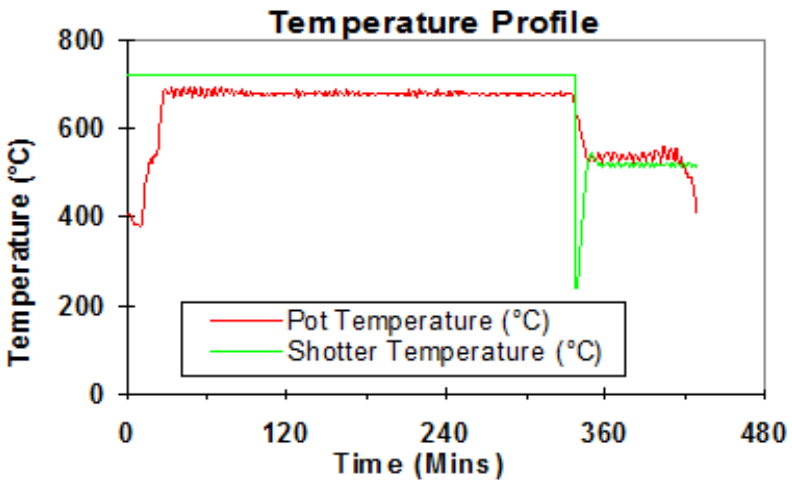

Figure 2.8. Temperature profile of Se-As master alloy synthesis.

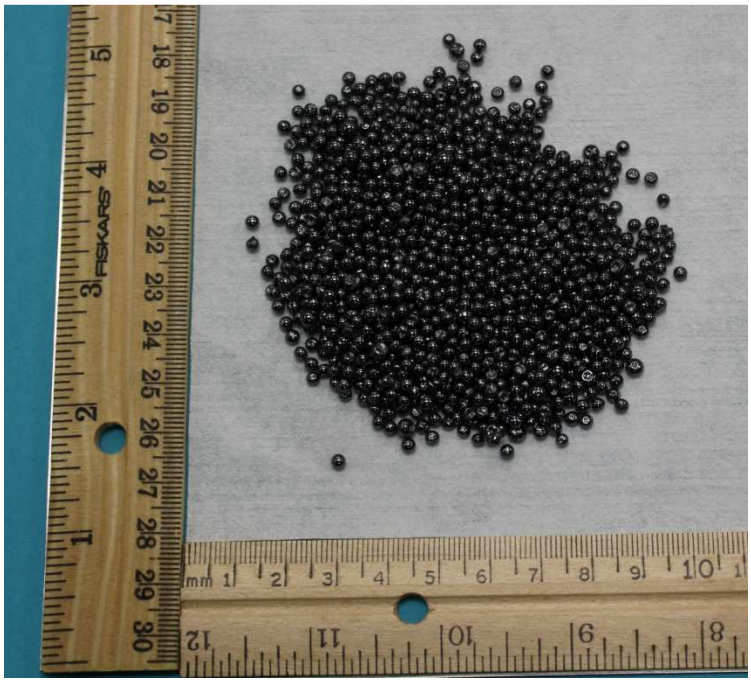

Figure 2.9. Sample#1 Se-As master alloy wet shots As-9.5%.

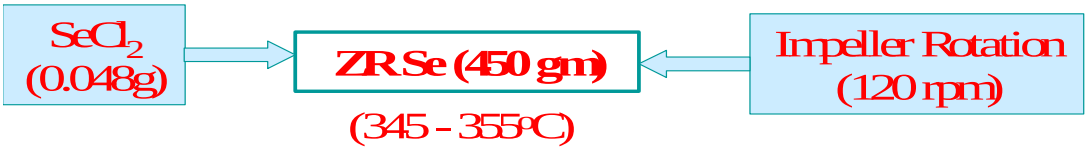

Figure 2.10. Synthesis of Se-Cl MS alloy

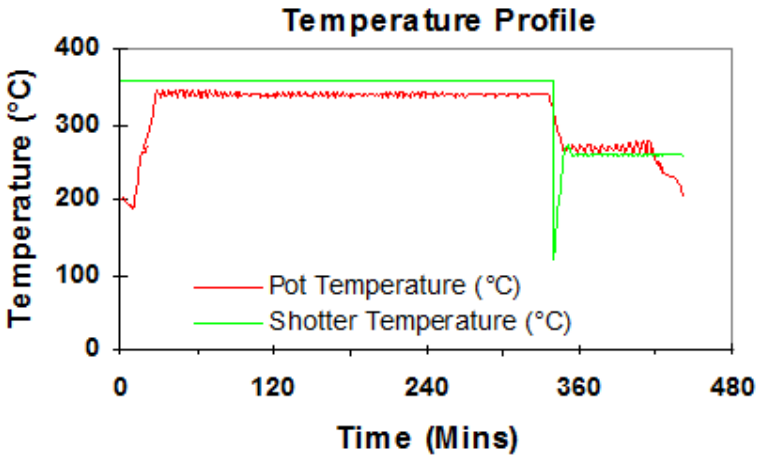

Figure 2.11. Temperature profile of Se-Cl master alloy synthesis.

Figure 2.12. Sample#2 Se-Cl master alloy wet shots Cl-0.34%.

2.3.3 Alloy Synthesis a-Se (As 0.52%, Cl 5ppm)

Zone refined Se was thoroughly mixed and crushed with previously synthesized 9.5% Se-As master alloy and 50 ppm of Se-Cl master alloy. The alloy-processing synthesis route was conducted in a tightly argon-controlled glove box. The alloy reactor was heated in a controlled manner to about 475^{o}C (~ 5.5 hours) and homogenized by a rotating impeller (425 rpm). The melt was cooled to 340^{o}C and the shotting performed with a SS 316 shotter maintained at 345^{o}C on a shotter plate at 5^{o}C. The flow sheet diagrams of a-Se (As, Cl) alloy synthesis are presented in the Figure 2.13. The pictures of a-Se (As, Cl) alloy shots with varying As and Cl concentrations are presented in Figure 2.14 and Figure 2.15. The compositions of the various synthesized alloys were determined by Inductively Coupled Plasma Mass Spectrometry (ICP/MS) analysis. In an ICP/MS system high-temperature ICP source converts the atoms of the elements in the sample to ions. These ions are then separated and detected by the mass spectrometer [38]. The composition determined by ICP/MS for different a-Se alloys are presented in Table 2.3.

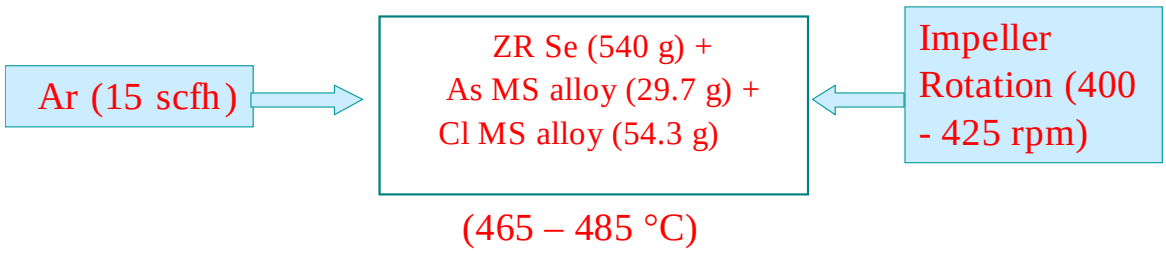

Figure 2.13. Synthesis of a-Se (As, Cl) bulk alloy

Figure 2.14. Sample #4 a-Se (As 0.52%, Cl 5 ppm) alloy pellets.

Figure 2.15. Sample #3 a-Se (As 10.2%, Cl 60 ppm) alloy pellets.

Table 2.3. Compositions of Se-alloys by ICP/MS analysis.

Alloys	Elements	Concentration
a-Se-As	Se	Major
	As	9.42 ± 0.1%
a-Se-Cl	Se	Major
	Cl	49 ± 2 ppm
a-Se-As-Cl	Se	Major
	As	0.52 ± 0.01%
	Cl	5 ± 1 ppm

2.4 FABRICATION OF a-Se (As 0.52%, Cl 5ppm) ALLOY FILMS

After preparation and detailed analysis of the a-Se alloys, various alloy films of different thickness were deposited over aluminum and ITO coated glass substrates. It is very important to carefully control the thin film deposition process. Substrates have to be prepared before a-Se can be deposited. This preparation step insures surface uniformity and improved adhesion. We have used ITO coated TEC-8 glass substrates. (25 cm^2) and aluminum oxide substrates. Oxidized aluminum (Al) substrates were used as aluminum oxide acts as p-like layer which blocks the injection of electrons from the respective negatively biased electrode.

2.4.1 Substrate preparation

The ITO coated glass substrates were rinsed in ethanol for 2 min, followed by acetone for 2 min and then sonicating with isopropanol. Finally they were rinsed in deionized water and drier under nitrogen.

The Al substrates were cut to desired sizes (1″ × 1″, 1.5″ × 1.5″, 2″ × 2″, and 4″ × 4″). To get rid of the unwanted impurities on its surface, the substrates were then ground, lapped and polished successively by fine emery paper, zirconium oxide powder, and fine alumina powder of various grain sizes down to 0.3 µm. At this point the Al surface had a near mirror finish. Then, the Al substrates were etched for 2 minutes with an etchant (H_3PO_4 : CH_3COOH : HNO_3 : H_2O = 4:4:1:1 by volume) and rinsed with Deionized water. After etching, most of surface defects were removed. Figure 2.16 shows the scanning electron microscopy (SEM) images of smooth surface of prepared Al substrates at different magnifications. Finally, the substrates were oxidized in a furnace by heating them at 350°C for 3 hours in air. After the subsequent etching and oxidation, the surface of the Al substrates became whitish instead of a dark gray color. This whitish color is representative of the presence of aluminum oxide. This substrate preparation step is critical because poorly prepared substrates result in large leakage currents.

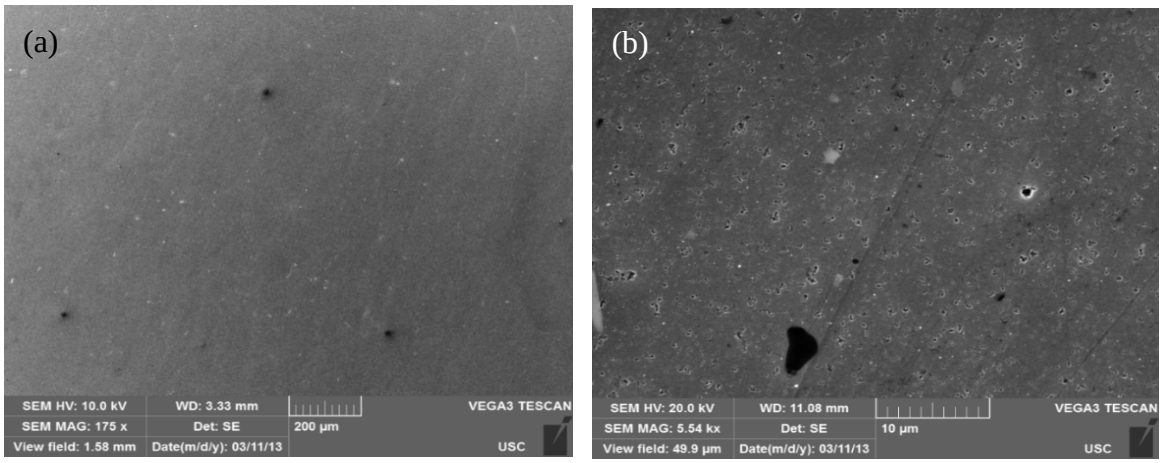

Figure 2.16. SEM image of prepared Al surface (a) at 175 x magnification and (b) at 5.54 K x magnification.

2.4.2 Film preparation

After substrate preparation, thin film deposition was carried out using our thermal evaporation facilities using a CHA SE 600 evaporator. Figure 2.17 shows the schematic of the thermal evaporator system used for a-Se (As,Cl) alloy film preparation. This evaporator is equipped with planetary rotation system and high vacuum pressure of $2x10^{-8}$ Torr can be achieved. Vacuum fixtures and substrate temperature accessories were installed within the thermal evaporation system. Deposition of a-Se necessitates a substrate temperature of 60-65^{o}C so that the resulting film will be amorphous.

Film depositions in the thermal evaporator were monitored by a quartz crystal thickness monitor. Usually a test sample is placed with the depositions and the corresponding film thicknesses was measured by Dektak IIA surface profilometer.

First the substrate is loaded on to the planetary rotating discs where they are held by thin tungsten wires placed on the edges. The desired alloy is then measured and loaded in a molybdenum boat. Up to three different boats can be simultaneously loaded in the thermal evaporator but in our depositions we usually used a single boat.

The vacuum chamber was evacuated to about 2×10^{-6} Torr and the chamber temperature was raised to 100°C in order to get rid of any moisture. After about 5 mins at 100°C, the chamber was allowed to cool down to 60°C which also represents the substrate temperature. For film deposition, it is necessary to grow the films with precisely controlled substrate temperature so that the film grows with amorphous phase. Finally by controlling the boat power amorphous films up to ~300 μm in thickness were deposited. During deposition, the alloy film can be polycrystalline if the temperature of the film is above its crystallization temperature. Because the selenium alloy has a poor thermal

conductivity and has a lower glass transition temperature than conventional semiconductors, it is difficult to avoid the poly-crystallization if we deposit the film continuously for long time. Thus, we have continuously monitored the substrate temperature during deposition process. If the substrate temperature reached around 10°C below the transition temperature, the film was cooled down by turning off the power to the evaporation source. Then, the deposition was resumed when the substrate was sufficiently cooled down. By this way, we have been able to deposit films up to 300 µm thickness with complete amorphous structure.

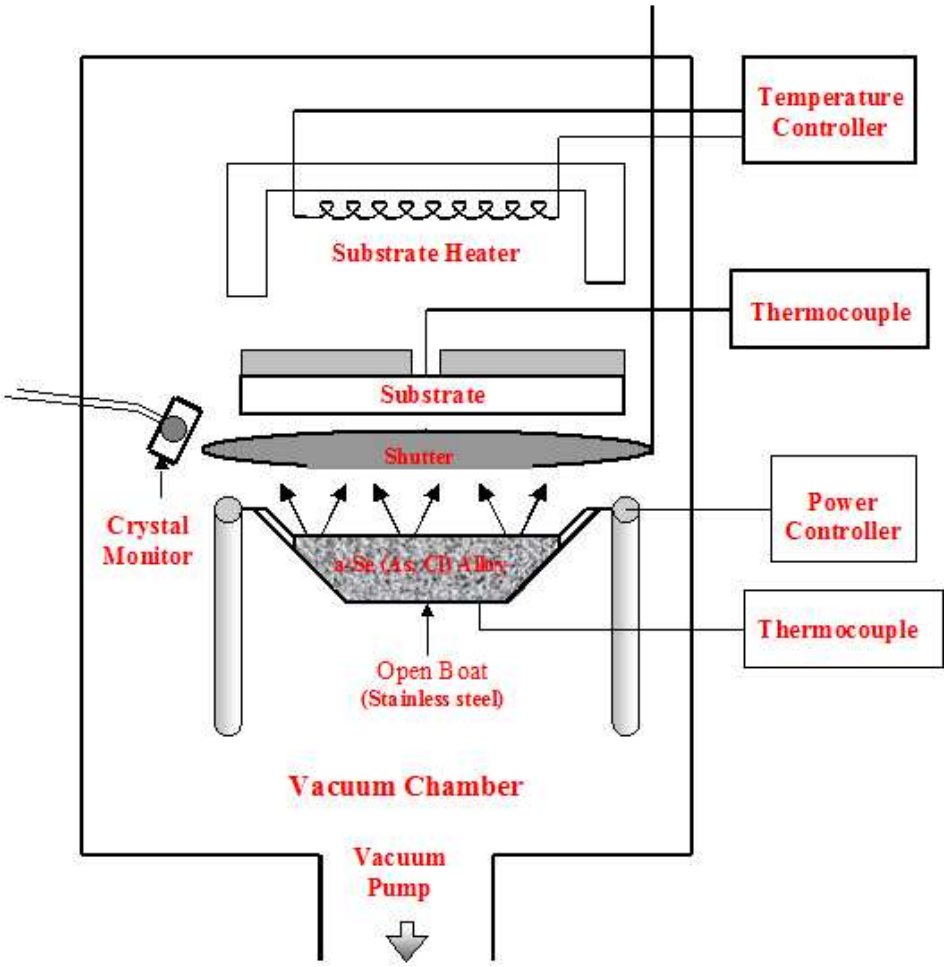

Figure 2.17. Thermal evaporator system and accessories.

The appearances of a-Se (As, Cl) alloy films are presented in Figure 2.18. The structural, physical, and electrical characterization of a-Se (As, Cl) films on ITO/Al substrates were carried out in details and described in Chapter 3. Evaluation of the surface morphology and composition was conducted using scanning electron microscopy (SEM) and X-ray diffraction (XRD) was used to confirm amorphous structure. The optical absorption study was conducted to estimate the bandgap energy (E_g). Resistivity and leakage current of the film was estimated from the current-voltage analysis.

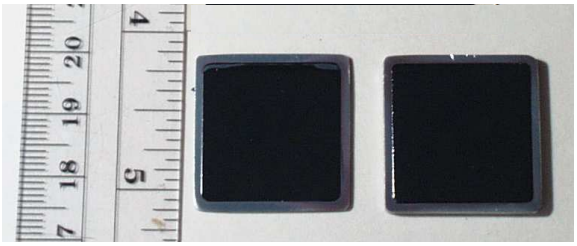

Figure 2.18. Amorphous Se (As, Cl) alloy films on 1” x 1” Al substrates.

2.5 CONCLUSION

In this chapter firstly purification by zone refining technique is reviewed and the effectiveness of this technique is analyzed by glow discharge mass spectroscopy. Secondly the purified Se materials were alloyed with As and Cl in the desired compositions and amorphous alloys were synthesized. The compositions of the synthesized alloys were characterized by ICP/MS analysis. In the following chapter these alloys will be further characterized to understand their optical, electrical and spectroscopic properties. Also in chapter 4 boron doped alloy synthesis is discussed that uses similar alloying principles.

CHAPTER 3: CHARACTERIZATION OF AMORPHOUS SELENIUM ALLOYS AND ALLOY FILMS

3.1 OVERVIEW

Various characterizations have been performed in order to study and verify the desired physical, electrical, optical and spectroscopic properties of the synthesized alloys. In order to understand the structural properties of the alloys they were characterized by x-ray diffraction and raman spectroscopy. Optical absorption study was performed to obtain band gap of the alloys. The a-Se alloys were surveyed by x-ray photoelectron spectroscopy to examine for any compound formation and impurities. Finally current-voltage measurements were performed to find the electrical resistivity of the alloys.

3.2 X-RAY DIFFRACTION

In order to get a diffraction pattern, the ground a-Se powder is bombarded with x-rays. When these x-rays interact with the material they either get diffracted or transmitted. Now because of unique physical properties like composition, lattice spacing and arrangement, the incoming beam gets diffracted at characteristic angles. Intensity versus angle plot is measured to determine the corresponding material. The wavelengths of the x-rays used in these experiments vary from 10 to 100 angstrom.

XRD was carried out for a-Se samples at different alloying stage. For each sample, first a mortar and pestle was used to grind the sample into a fine powder and then pressed to obtain a-Se pellets as shown in Figure 3.1. The x-ray diffraction pattern was

obtained using a Rigaku D/MAX 2100 Powder X-ray diffractometer (CuKα radiation, λ = 0.15406 nm). XRD study was first carried out for zone-refined Se precursor material. Samples from both ends – pure and impure – were analyzed and the data are presented in the Figure 3.2. The data shows that the precursor Se material was polycrystalline in nature as evident from the characteristic diffraction peaks.

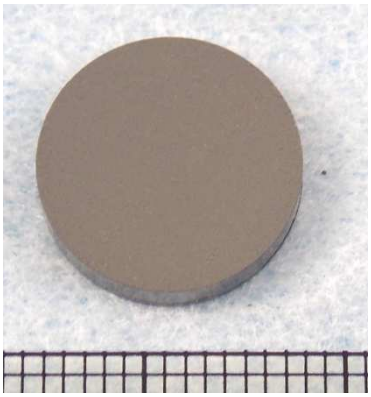

Figure 3.1. Standard Ground and pressed a-Se pellets (2mm thick and 13 mm in diameter) used for XRD characterization.

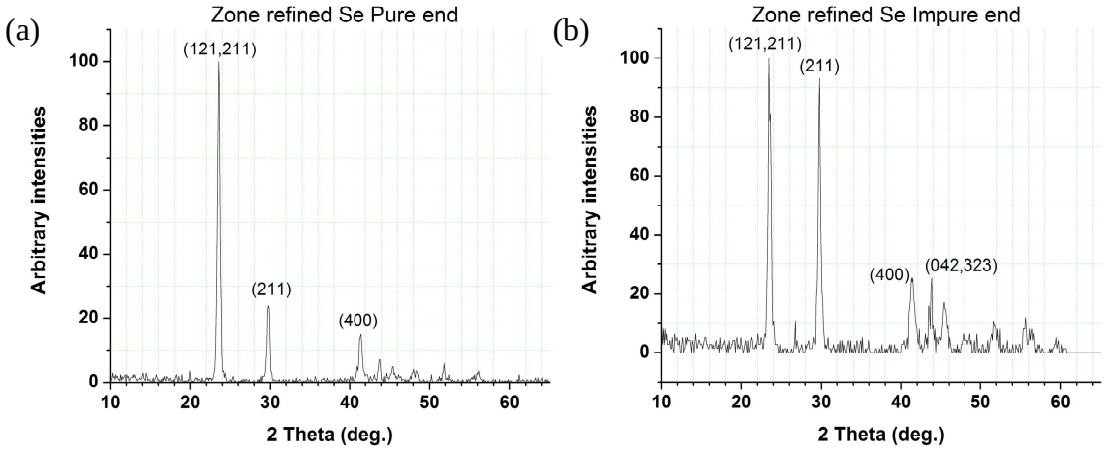

Figure 3.2. (a) XRD pattern of pure end of zone refined selenium. (b) XRD pattern of impure end of zone refined selenium.

Powdered a-Se (As, Cl) alloys were then characterized by X-ray diffraction. A typical XRD pattern of the powdered a-Se (As, Cl) alloy is shown in Figure 3.3. From the X-ray diffraction pattern is can be observed that diffraction peaks because of compound formation, extraneous phases or segregation are not present [39]. Hence the XRD confirms the amorphous structure of the stabilized a-Se (As 0.52%, Cl 5 ppm) alloy.

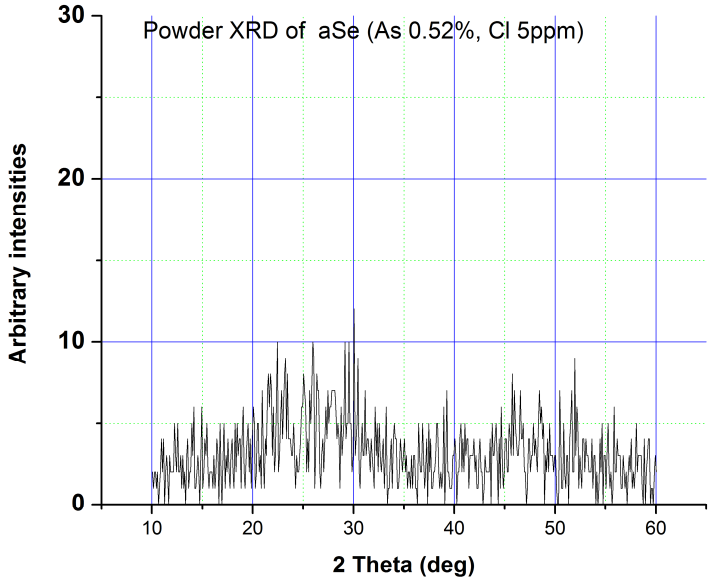

Figure 3.3. XRD pattern of a-Se (As 0.52%, Cl 5 ppm) alloy.

An XRD pattern of a-Se (As 0.52%, Cl 5 ppm) thin film on ITO coated glass is shown in Figure 3.4. There are no diffraction peaks identifiable for any major or minor crystallographic orientation. The observed diffraction pattern corresponded very well to the standard x-ray pattern for Se alloys with amorphous structure. No other peaks due to impurities or any other phases were observed within the sensitivity of the instrument (0.1%). Thus XRD confirmed that a-Se with an As content of ~0.52% and Cl content of ~5ppm is totally resistant to crystallization.

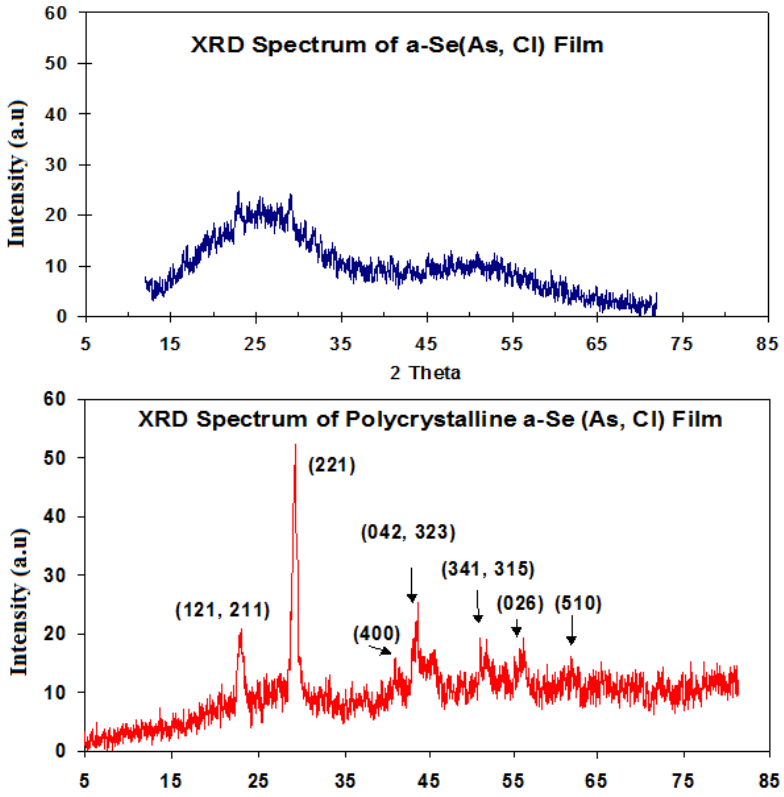

Figure 3.4. XRD patterns of amorphous (top) and polycrystalline (bottom) a-Se (As 0.52%, Cl 5 ppm) alloy films.

3.3 SURFACE MORPHOLOGY STUDIES

Scanning electron microscope (SEM) typically works by bombarding the semiconductor sample surface with focused beam of high-energy electrons. When these electrons interact with atoms in the sample, they produce various signals that are detected and they contain information about the sample's external morphology (texture), chemical composition, and crystalline structure and orientation. In most applications, data are collected over a selected area of the surface of the sample, and a 2-dimensional image is generated that displays spatial variations in these properties [40].

SEM studies were carried out at the Electron Microscopy Center of USC. Amorphous Se (As, Cl) alloy samples were prepared for SEM analysis using the following sample preparation steps. The surface of the 1 inch × 1 inch × 0.33 mm aluminum (Al) substrate was cleaned and polished by fine alumina powder – of 1 micron followed by 0.3 micron grain size - for a mirror finish and then etched with etchant. Then the substrate was cleaned successively with acetone, isopropanol and DI water, and dry cleaned with an ultrasonic vapor degreaser. On the clean, scratch-free surface of Al-substrate, a-Se (As, Cl) alloy film was deposited by thermal evaporation. Details of the film deposition processes are described in the Section 2.4. A gold (Au) top contact of about 50 nm was sputtered by a DC sputtering unit. The conductive gold coating prevents charge build-up on the a-Se sample during high resolution electron imaging applications. The microscopic surface morphology of the alloy film is presented in Figure 3.5 that reveals smooth and shiny surface with no pinholes, deep scratches or major defects.

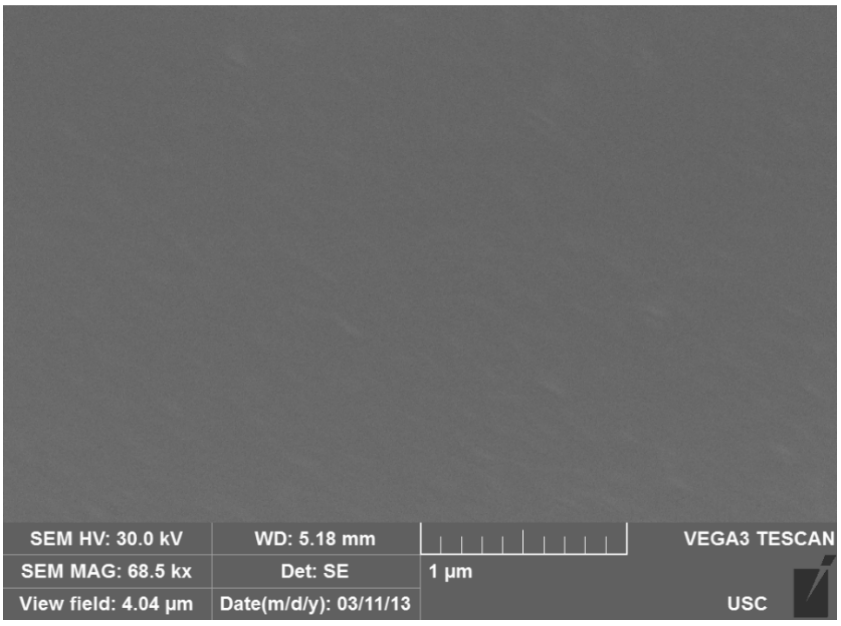

Figure 3.5. SEM image of a-Se (As 0.52%, Cl 5 ppm) alloy surface on Al-substrate.

3.4 RAMAN SPECTRSCOPY

Raman spectroscopy is a spectroscopic technique used to observe vibrational, rotational, and other low-frequency modes in a system. It relies on inelastic scattering, or Raman scattering, of monochromatic light, usually from a laser in the visible, near infrared, or near ultraviolet range. The laser light interacts with molecular vibrations, phonons or other excitations in the system, resulting in the energy of the laser photons being shifted up or down. The shift in energy gives information about the vibrational modes in the system.

Typically, a sample is illuminated with a laser beam. Light from the illuminated spot is collected with a lens and sent through a monochromator. Wavelengths close to the laser line due to elastic Rayleigh scattering are filtered out while the rest of the collected light is dispersed onto a detector.

Raman spectra were recorded in a Horiba-Yvon LabRam HR800 system in backscattering geometry and confocal configuration. A 784-nm diode laser with a power density of 1 W/cm^2 was used as the light source. Amorphous Se samples with different doping concentrations of As and Cl were analyzed by the Raman Spectroscopy. The details of these samples are specified in the following list.

Sample ID	Sample Specifications
S 0727O	a-Se-As master alloy
S 0727G	a-Se-Cl master alloy
S 0727R	a-Se (As 0.52%, Cl 5ppm) alloy
S0727Y	a-Se (As 10.2%, Cl 60 ppm) alloy

Figure 3.6 shows room temperature Raman spectra of a-Se related samples. It is seen that the spectra of a-Se-As master alloy (S 0727O) and a-Se (As 0.52%, Cl 5ppm) alloy (S 0727R) are almost identical. Seven vibrational modes located at 40(41), 59(60), 77, 110, 133, 228 and 251 cm^{-1} are found. Compared with the spectrum of S 0727R, spectrum of a-Se (As 10.2%, Cl 60 ppm) alloy S0727Y possesses one more peak and one more shoulder located at 216 and 205 cm^{-1}. The spectrum a-Se-Cl master alloy (S 0727G) seems to be different from others. Only two vibrational modes located at 142 and 234 cm^{-1} were found.

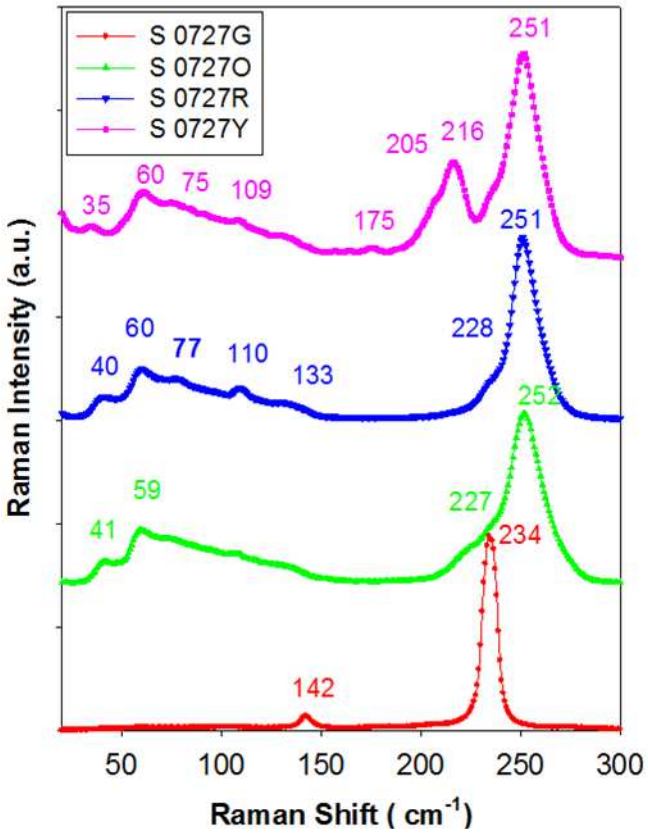

Figure 3.6. Room temperature raman spectra of amorphous selenium samples excited with 784 nm laser.

The Raman spectra of a-Se in metastable monoclinic form were reported by Lukovsky [41] and Gorman [42]. Lukovsky found characteristic vibrational modes at 50, 80, 112, 138, 235 and 250 cm^{-1}; while Gorman gave the corresponding modes at 80, 110, 132, 234 and 250 cm^{-1}. Among them the 112 cm^{-1} was regarded as Se_8 ring and ring like species in the amorphous structure [43, 44].

The 235 cm^{-1} mode, was linked to the trigonally crystalline Se chain structure. Thus the absence of the 235 cm^{-1} mode in the samples S 0727O and S 0727R , which are a-Se (As,Cl) alloy materials, indicates that trigonally crystalline Se chain structure is not present. Peak at 251cm^{-1} is related to helical and string chains of the structure present in amorphous selenium. This peak was present in both S 0727O and S 0727R a-Se (As,Cl) alloy samples and agrees with the published literatures [45, 46]. Therefore, amorphous state was confirmed for the samples S 0727O and S 0727R. The sample S0727 G (a-Se-Cl master alloy) was unstable form of trigonal structure as confirmed by other researchers [47, 48].

Figure 3.7 shows temperature dependence of Raman spectra for a-Se (As 0.52%, Cl 5ppm) alloy sample (S 0727R). Temperature effect on the vibration modes of the sample is found insignificant. It is observed that the Raman intensity decreased with decreasing temperature (as expected), however, Raman shift was very small. All modes shifted slightly to lower values at higher temperature (less than 1 cm^{-1} from 77 K to RT).

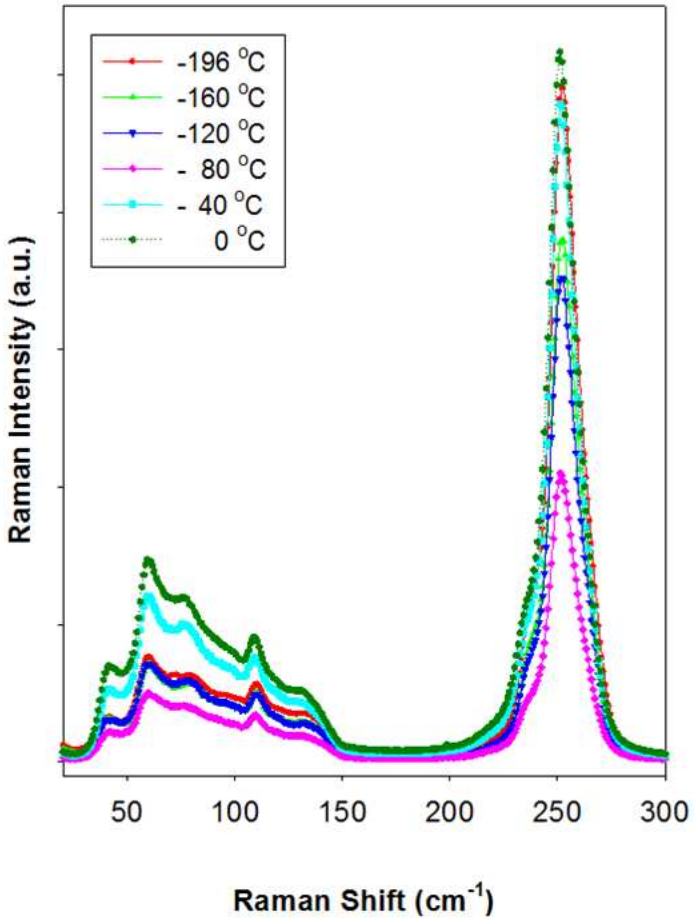

Figure 3.7. Temperature dependence Raman spectroscopy of the sample S 0727R - a-Se (As 0.52%, Cl 5ppm) alloy.

3.5 DIFFERENTIAL SCANNING CALORIMETRY

Differential Scanning Calorimetry (DSC) measurements were performed in TA Q200 system. DSC measures the temperatures and heat flows associated with transitions in materials as a function of time and temperature in a controlled atmosphere. These measurements provide quantitative and qualitative information about physical and chemical changes that involve endothermic or exothermic processes, or changes in heat capacity. We have used this technique to determine the melting points and the heat of fusion (HF) for the a-Se alloy samples [49].

For our investigation, the heating rate was kept at 10 ^{o}C/min. DSC analysis was carried out for the four a-Se alloy samples with various As and Cl concentrations. Figure 3.8 shows typical DSC curves of heat flow with varying temperature. The melting point was determined from the onset of a valley and the heat of fusion was determined from the area under the respective valley. For S 0727G (a-Se-Cl master alloy), the melting point (MP) is found to be 219.6°C and the heat of fusion is calculated to be 75.0 J/g. S 0727O (a-Se-As master alloy), the MP is 98.7°C; the HF is 109.3 J/g. For S 0727R which is a-Se (As 0.52%, Cl 5ppm) alloy, the glass transformation temperature is 50.0^{o}C, M.P is 215.3°C, and the HF is 55.2 J/g. For S 0727Y which is a-Se (As 10.2%, Cl 60 ppm) alloy, the values are slightly higher as expected. For this alloy the glass transformation temperature is 56.6 ^{o}C, the MP is at 225.3°C and the HF is 75.4 J/g. These data are in agreement with the data published by Holubova et al. [48].

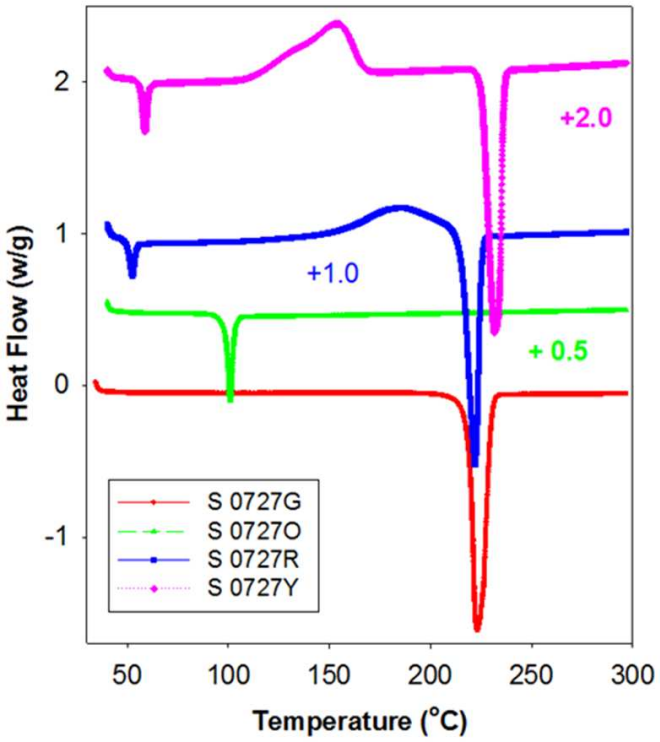

Sample ID	Sample Specifications
S 0727G	a-Se-Cl master alloy
S 0727O	a-Se-As master alloy
S 0727R	a-Se (As 0.52%, Cl 5ppm) alloy
S0727Y	a-Se (As 10.2%, Cl 60 ppm) alloy

Figure 3.8. DSC trace scan at 10°C/min of a-Se alloys

3.6 Optical Absorption Studies on a-Se (As,Cl) Alloy Films

The analysis of optical spectra over a wide range of photon energy has been one of the most productive tools for understanding and developing the theory of electronic structure in crystalline and amorphous solids. The optical absorption studies were conducted on B-doped a-Se (As, Cl) alloy films on ITO glass substrate. Figure 3.9 shows a typical optical absorption ($\hbar\alpha\upsilon$) vs. incident photon energy ($\hbar\upsilon$, eV) curve. An ITO coated glass slide was used as the reference, and the values of optical absorption coefficient (α) were not corrected for the reflection of the alloy surface. The energy bandgap (E_g) was estimated by extrapolating the linear region of the curves to $(\hbar\alpha\upsilon)^{1/2} = 0$ [50], and the value of E_g was estimated to be about 2.21 eV at 300K which is in close agreement with other a-Se based alloys [17, 25].

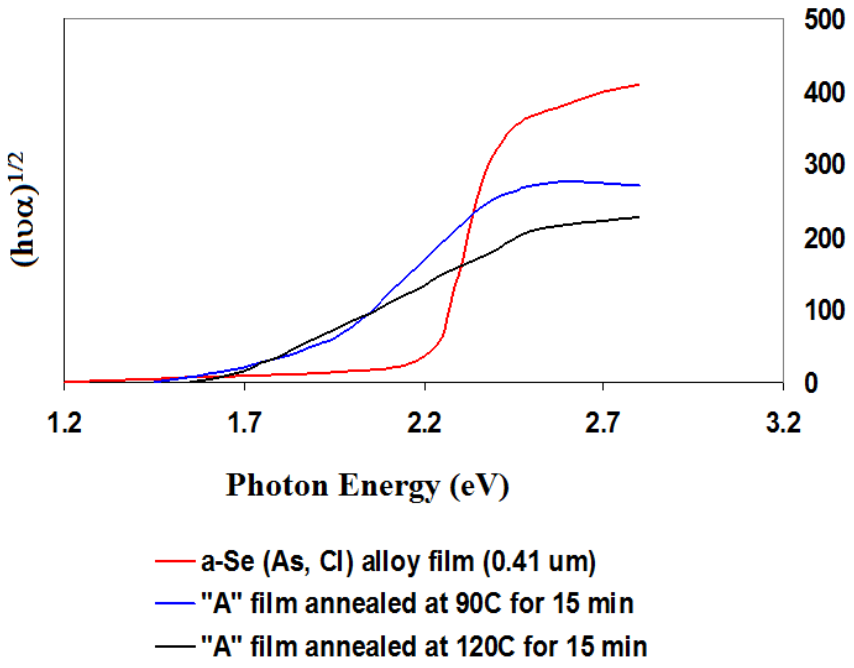

Figure 3.9. Optical absorption studies.

3.7 X-RAY PHOTOELECTRON SPECTROSCOPY SURVEY SCAN

The XPS survey scans on a-Se (As, Cl) alloy material was carried out to examine As, and Cl concentrations at the surfaces and to examine presence of any compound formation and other impurities. The XPS investigations were carried out using a Vacuum Generator ESCALAB MKII equipped with XPS/Auger spectrometer with a MgKα source (E=1253.6 eV) with 300 W power at 15 KV. Data acquisition and analysis for XPS used a Physical Electronics multiple technique analytical computer system. The peak energies were measured after the data were smoothed. Figure 3.10 represents a typical XPS survey scan for a-Se (As, Cl) alloys. The observed binding energies for Se, As and Cl are in the correct range as found in the literature [46]. Other than unavoidable peaks of oxygen and carbon there are no peaks for impurities.

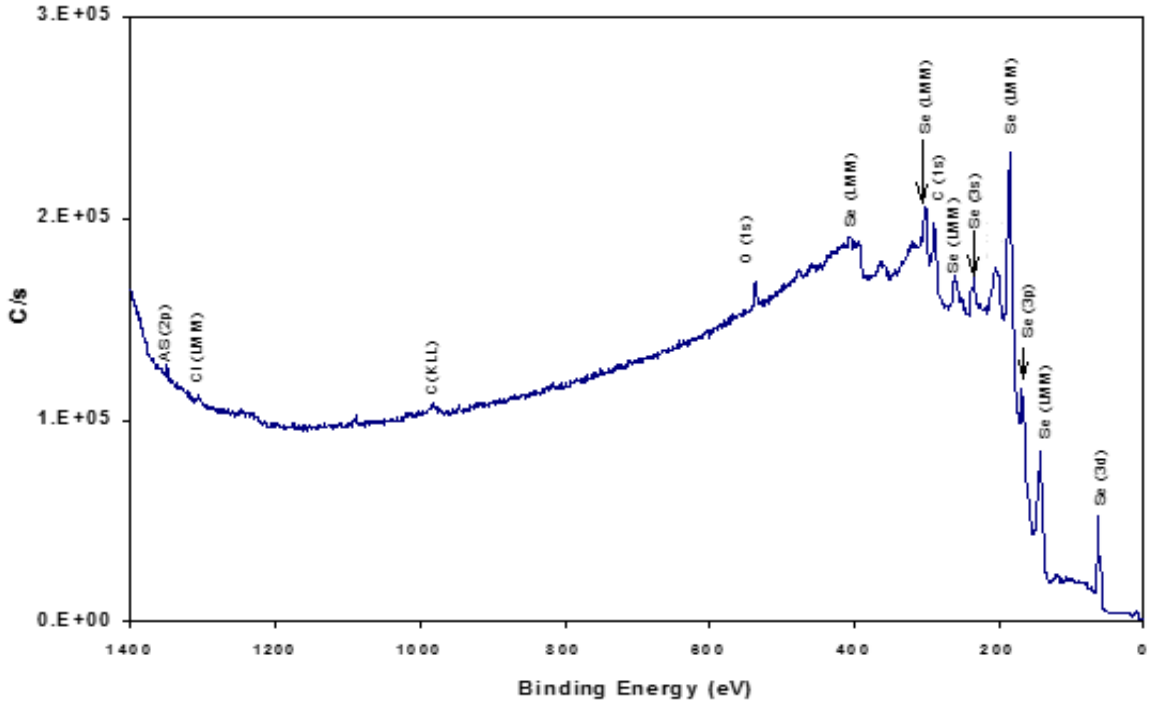

Figure 3.10. XPS survey scan on a-Se (As, Cl) alloy wafer.

3.8 ELECTRICAL CHARACTERIZATION

Current-voltage measurements were performed to evaluate the resistivity of various a-Se alloys in order to determine their usability as radiation detectors.

3.8.1 Device Fabrication

The a-Se (As, Cl) alloy films of 6.25 cm^2 in area on aluminum substrate were used for device fabrication. Metal contacts were deposited on the top surfaces of the alloy films using metallization shadow mask technique. The bottom contact was oxidized aluminum and the top contact was semitransparent gold of thickness 6-10 nm deposited by DC sputtering. Thin copper wires were attached with silver epoxy and the contact area (0.03 cm^2) was encapsulated with very thin epoxy adhesives. The fabricated devices with different sizes of top gold contact are presented in Figure 3.11 and Figure 3.12.

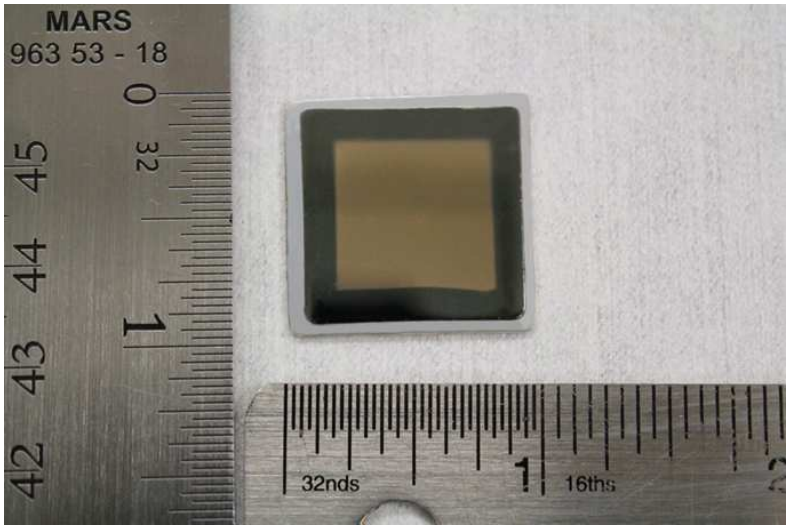

Figure 3.11. Al/a-Se(As,Cl) alloy/Au film #1.

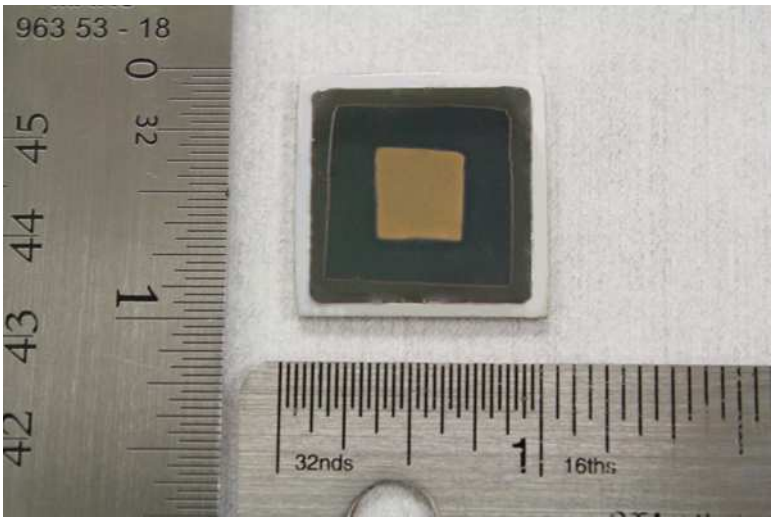

Figure 3.12. Al/a-Se (As, Cl) alloy/Au film #2.

3.8.2 Current-Voltage Measurements

In order to perform the I-V characterization of amorphous selenium samples, a shielded aluminum box was used to hold the samples and protect them from electrical interferences. As shown below the box contains a connector to interface the sample with Keithley 237. The sample is placed on top of a conducting stage which contains a bottom contact and a thin strip of copper, which touches the top of the sample, and acts as the top contact.

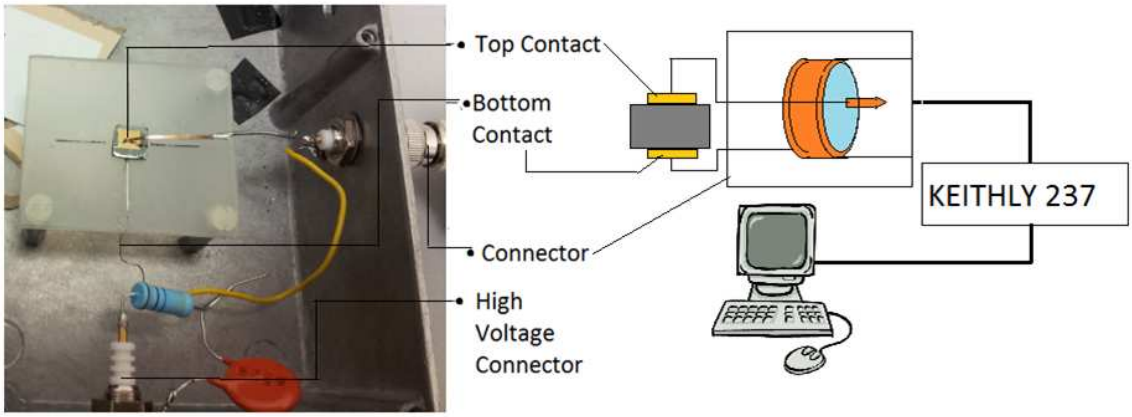

When a voltage is applied, current flows through the a-Se alloy film device. This relationship is used to measure the dark current i.e. the current flowing through the alloy in the absence of irradiation. This experiment was performed at room temperature and on a vibration free table. From Ohm's Law resistance of the sample is determined which is the inverse of the calculated slope of the I-V plot. The resistivity is calculated using the following equation:

$$\rho = R \cdot \frac{A}{L}$$

Where ρ is the resistivity of the a-Se alloy in Ohm-cm, R is the resistance in Ohms, A is the contact area (cm^2), and L is the thickness (cm) of the a-Se alloy.

Current-voltage (I-V) plot of different a-Se samples are presented in Figures 3.13 – 3.16, and the calculated resistivity and resistance of the samples are summarized in Table 3.1. The measured resistivity was estimated to be about $2x10^{14}$ Ω.cm for a-Se (As 0.52%, Cl 5ppm) alloy films whereas that for a-Se (As 10.2%, Cl 60 ppm) alloy film was $6.5x10^{10}$ Ω.cm. Therefore, a-Se (As 0.52%, Cl 5ppm) alloy material, which is highly amorphous, showed very high resistivity as required for radiation detector applications. The dark (or leakage) current density was also very low for the above alloy composition - only a few pA/cm^2. No hysteresis were observed for the a-Se (As, Cl) alloy materials showing minimal charge recombination or trapping.

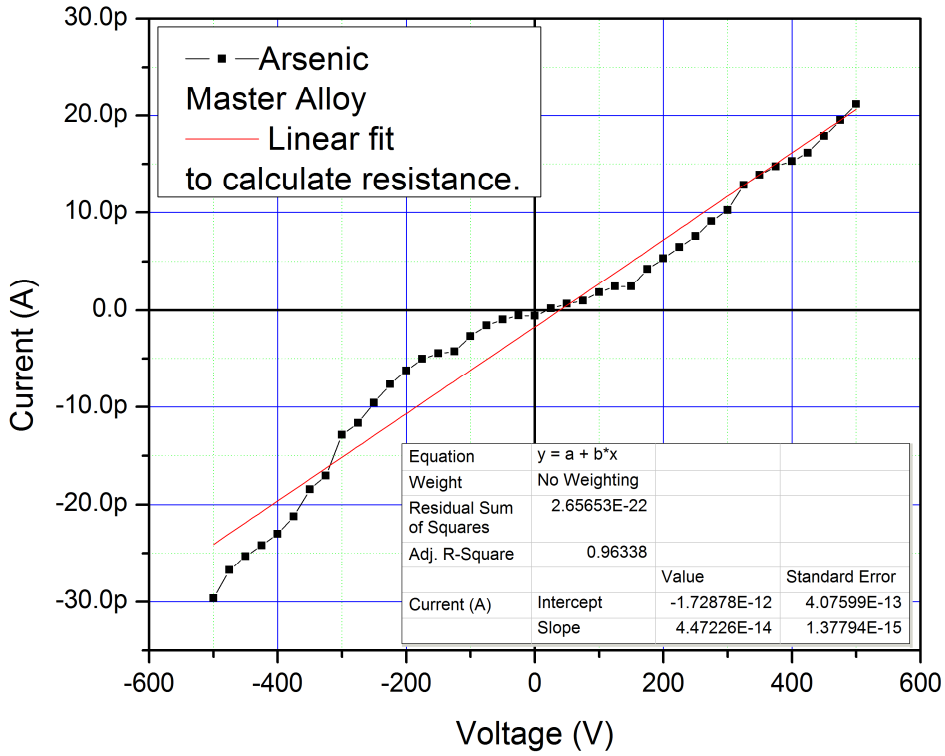

Figure 3.13. Current (I)-voltage (V) characteristics and linear fit calculations of Arsenic-Selenium master alloy.

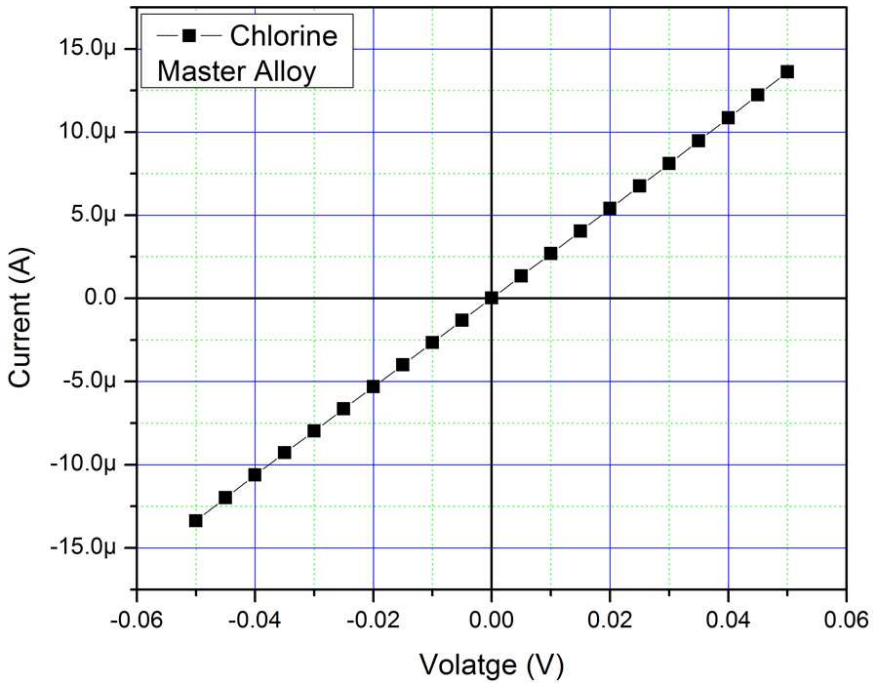

Figure 3.14. . Current (I)-voltage (V) characteristics of Chlorine-Selenium master alloy.

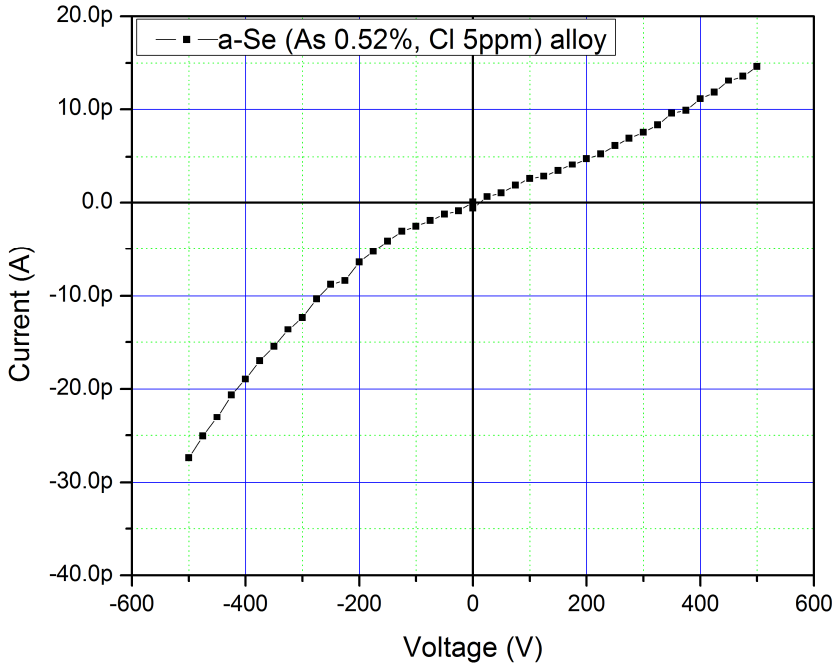

Figure 3.15. Current (I)-voltage (V) characteristics for a-Se (As 0.52%, Cl 5 ppm) alloy device. No hysteresis were observed showing minimal charge recombination or trapping.

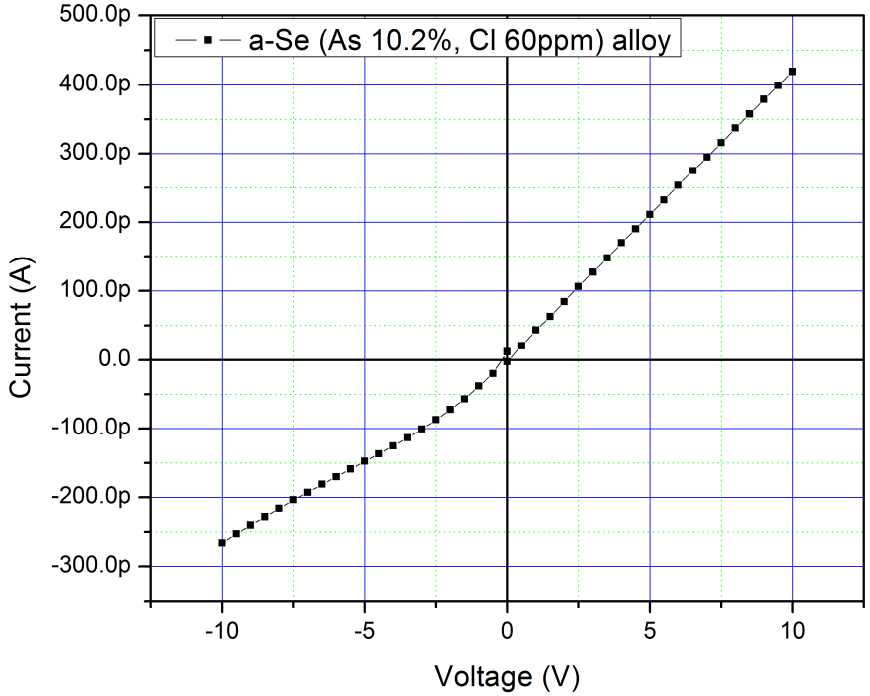

Figure 3.16. Current (I)-voltage (V) characteristics for a-Se (As 10.2%, Cl 60 ppm) alloy device.

Table 3.1. Resistivity of characterized a-Se alloys.

Sample	Voltage range (V)	Current range (pA)	Mean Resistance (Ω)	Resistivity (Ω-cm)
Se-As master alloy wet shots (As: 9.5%)	Min=-500 Max=500	Min=-29.6 Max=21.16	2.236×10^{13}	5.3×10^{13}
Se-Cl master alloy wet shots (Cl: 0.37%)	Min=-0.05 Max=0.05	Min=-13.37 Max=13.61	3.72×10^{3}	15.7
a-Se (As 0.52%, Cl 5 ppm) alloy	Min=-500 Max=500	Min=-27.41 Max=14.63	2.725×10^{13}	1.96×10^{14}
a-Se (As 10.2%, Cl 60 ppm) alloy	Min=-10 Max=10	Min=-266 Max=419	2.864×10^{10}	6.52×10^{10}

3.9 CONCLUSION

The characterization results show that the properties of synthesized alloys are in the desirable range and can be potentially utilized to make detector grade devices. Particularly it is very promising to find that the synthesized alloys are amorphous and the fabricated devices are highly resistive. The alloy films have good surface properties and free from parasitic defects. Also physical properties like melting point, crystallization temperature, bandgap energy, etc. are in agreement with what is found in the literature.

CHAPTER 4: BORON-DOPED SELENIUM ALLOY SYNTHESIS AND CHARACTERIZATION FOR NEUTRON DETECTION APPLICATION

4.1 OVERVIEW

After extensive characterization of a-Se alloys, highly resistive and amorphous in nature a-Se (As 0.52%, Cl 5ppm) alloy material were chosen for boron (B) doping in order to develop a new room temperature direct-readout solid-state thermal neutron detector. The synthesis of natural isotropic boron (^{10}B) doped a-Se (As, Cl) alloy materials were carried out using a special pelletizing apparatus designed and constructed for this purpose. After synthesis, the compositions of the alloy material were determined by ICP/MS analysis. B-doped alloy films were then characterized for their morphological (SEM studies), optical (XPS and photosensitivity), and electrical (current-voltage) properties. These results provided the data required to demonstrate the benefits of this new neutron detector and identify the areas that require further research in future.

4.2 PHASE DIAGRAM OF THE BORON-SELENIUM SYSTEM

The phase diagram of the B-Se system as presented in Figure 4.1 shows that the thermodynamics of B alloy formation has a major problem associated with:

1. An immiscibility-gap on the selenium rich side,
2. Formation of B_2Se_3 which is very stable and has a very low vapor pressure, and
3. The activity coefficient of B in the B-Se system is very low and hence so is the partial pressure of boron.

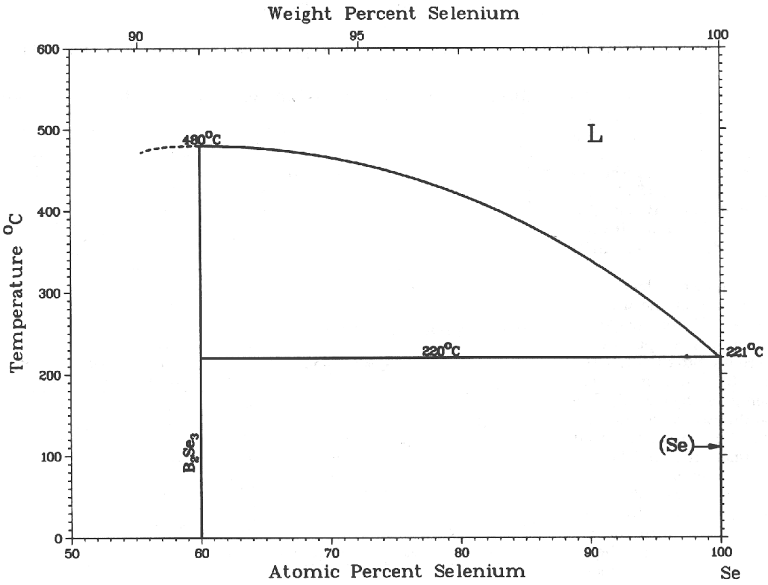

Figure 4.1. The phase diagram of B-Se system.

We have overcome these problems by: (i) heat treating the alloy melt at elevated temperature of 475°C for a short period of time (15 min.), and (ii) by preparing two different concentrated alloys of mono-dispersed boron in a-Se (As, Cl) matrix to increase the activity coefficient of boron. The key was to avoid the reaction of boron and selenium and successively increase boron concentrations in pre-synthesized alloys.

4.3 SYNTHESIS OF BORON DOPED A-SE (AS, CL) ALLOYS

Boron-doped a-Se (As, Cl) alloy materials was prepared using the same pelletizing alloy reactor as used to synthesize a-Se alloys and as shown in Figure 2.6. For a typical alloying process run, about 300 g of a-Se (As 0.52%, Cl 5ppm) alloy was loaded to the alloy reactor and 9.2 g of elemental boron (natural isotopic B, 300-mesh size) was added slowly. The process cycle was operated in a glove box maintained in a pure argon atmosphere. The alloy reactor was heated in a controlled manner to 465°C for 5 hours and homogenized by a rotating impeller (1200 rpm). The melt was cooled to 355°C and

shotting was performed with Stainless Steel 316 shotter maintained at 360^{o}C on a shotter plate at 5^{o}C. When the melt reached the shotting plate, it was quenched due to rapid decrease of temperature and it formed an amorphous phase. The alloying parameters such as height (dynamic relaxation effect) of a-Se (B, As, Cl) liquid melt in the shotter, synthesis temperature vs. time, and shotting plate temperature are very important and were observed closely.

A typical temperature profile with alloying time for one process run is presented in Figure 4.2, and the physical appearance of the synthesized B-doped a-Se (As, Cl) alloy is shown in Figure 4.3. The synthesized alloy has a dark color with shiny surface on one side. The preparation conditions of B-doped (natural isotopic boron) a-Se (As, Cl) alloy shots were optimized to obtain a-Se alloy with B up to 28 a/o. The compositions of the various synthesized alloys were determined by ICP/MS analysis and are presented in Table 4.1.

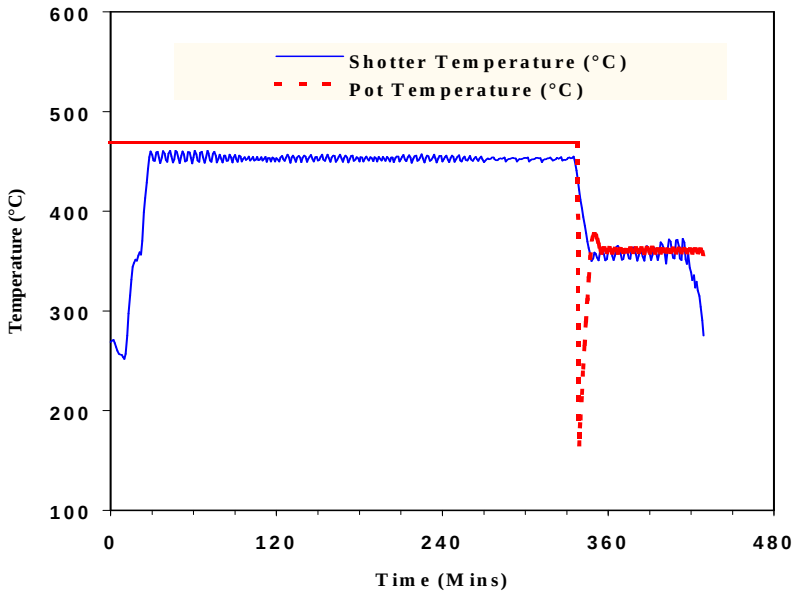

Figure 4.2. Temperature profile (Temperature vs. time characteristics) for B-doped a-Se (As, Cl) bulk alloy synthesis.

Figure 4.3. Enriched ^{10}B-doped Se (As, Cl) alloy dry pellets.

Table 4.1. Compositions of Se-alloy by ICP/MS analysis.

Alloys	Elements	Concentration
a-Se (B, As, Cl)	Se	Major
	B	18.4 ± 0.8 a/o
	As	0.51± 0.04%
	Cl	5 ± 2 ppm

4.4 SYNTHESIS OF BORON DOPED A-SE (AS, CL) ALLOY FILMS

B-doped a-Se alloy film deposition onto 1" x 1" Al and ITO coated glass substrates were carried out using thermal evaporation method. Aluminum substrates with 1/8" thickness and ITO/glass substrates with 0.5 mm thickness were pre-cleaned successively with acetone, isopropanol and DI water and were dried by immersing into an ultrasonic vapor degreaser. Aluminum substrate etching was conducted in a caustic

solution of sodium phosphate carbonate solution (for 3 min), and then dipped in concentrated nitric acid (for 2 min). The substrates were finally rinsed thoroughly with DI water. Then substrates were dried under a constant flow of N_2 gas.

B-doped a-Se (As, Cl) alloy films (≥ 300 μm thick) were prepared under a vacuum pressure of less than 10^{-6} Torr. Both the source (boat) and substrate temperatures were electronically controlled by microprocessor based temperature controller and the substrate temperature was maintained at $68^oC \pm 0.5^oC$. The source controller allowed temperature-time profile to be programmed for the evaporation cycle. The source was preheated to 280^oC at a rate of about 15^oC/min, and then kept at 280^oC, while the evaporation rate was adjusted to ~3.5 μm per minute. K-type thermocouples were used to read the temperatures of both source and substrate, which were maintained constant during the alloy film deposition process. The film deposition rate was precisely monitored using a quartz crystal thickness monitor. After synthesis to desired film thickness, the samples were allowed to cool-down to 30^oC before being removed from the evaporator.

4.5 X-RAY PHOTOELECTRON SPECTROSCOPY

The x-ray photoelectron spectroscopy (XPS) experiments were conducted using a Vacuum Generator ESCALAB MKII equipped with XPS/Auger spectrometer with a MgK_α source (E=1253.6 eV) with 300 W power at 15 KV. Data acquisition and analysis for XPS used a Physical Electronics multiple technique analytical computer system with Physical Electronics Version 6 software.

XPS was performed on the surfaces of B-doped a-Se (As, Cl) films. The survey scan corresponds very well with a-Se (B, As, Cl) alloying elements. There were no shifts

in binding energy, which indicates clearly the absence of any compound (e.g., B_2Se_3 or B_2SeO_4) formations. High-resolution XPS studies were conducted to identify structural coordinates. From the high-resolution XPS scan presented in Figure 4.4, the binding energy for Se 3d was found to be 55.4 eV and for As $3p_{3/2}$ and $3p_{1/2}$ was found to be 141.7 eV and 146.4 eV, respectively. These binding energies are in the correct range for a-Se (As, Cl) alloy as found in the literature [51]. Argon ion etching (5.0 KV; rate of sputtering 48 nm/min for Se) for 15 mins was conducted to determine the compositions along the cross-section of the films. Argon ion etching (Figure 4.4) also confirms the uniform distribution of alloying elements (B, As & Cl) from the surface towards the bulk depth up to 0.15 μm.

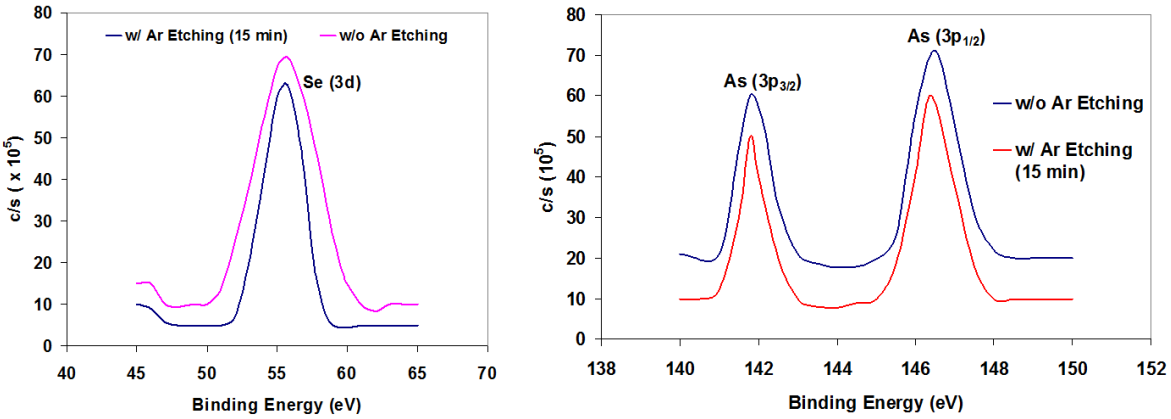

Figure 4.4. High-resolution photoemission spectra of ^{10}B-doped Se (As, Cl) alloy before and after argon (Ar) etching for 15 minutes.

4.6 PHOTOCURRENT CHARACTERISTICS

Photocurrent characteristics were measured to observe the photo-response of B-doped a-Se (As, Cl) alloy materials to lights of varying wavelengths. B-doped samples were tested for photosensitivity to wavelengths between 200 nm to 1000 nm, and the respective current was plotted at 5μW illumination for both polarities. The observed photocurrent characteristics are presented in Figure 4.5, which shows that B-doped a-Se samples were photosensitive at about 450 nm.

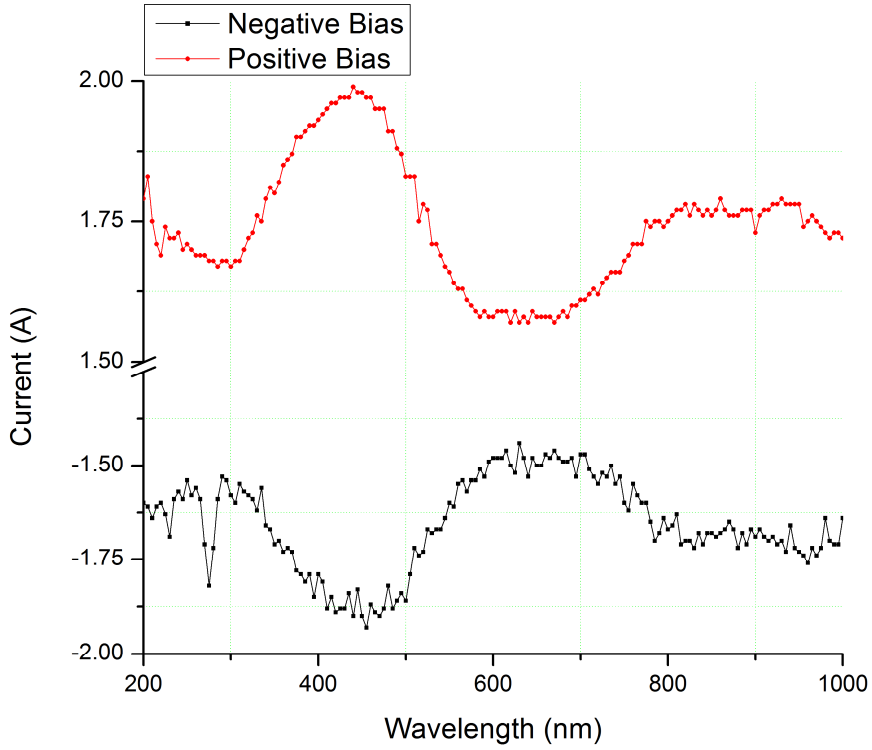

Figure 4.5. Photocurrent characteristics of B-doped samples biased at ±500 V.

4.7 CURRENT-VOLTAGE MEASUREMENTS

For this experiment, aluminum (Al) substrate used to deposit B-doped a-Se (As, Cl) film was first oxidized by heating at 220°C for about two hours. The aluminum oxide layer is important for the growth of B doped a-Se (As, Cl) films as it prevents dark current injection from the substrate as the aluminum oxide acts as a good blocking layer [52] and also aids the growth of uniform amorphous selenium layers. Semitransparent top gold contact was deposited by radio frequency sputtering (RF) process. Thin wires (copper or palladium) were attached with silver epoxy and the contact area was encapsulated with readily available epoxy adhesives (Dupont). A typical device based on B-doped a-Se(As, Cl) alloy is shown in Figure 4.6.

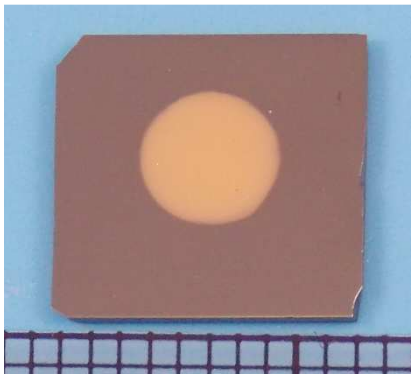

Figure 4.6. Boron doped a-Se alloy detector with top gold contacts of 4.5 mm diameter.

The current-voltage (I-V) measurements of B-doped a-Se alloy device was carried out at 20°C and 40°C (Figure 4.7) and corresponding resistivities have been calculated and summarized in Table 4.2. The current-voltage characteristics indicated high field penetration (i.e., strong charge carrier depletion region formation) into the devices and

high field tolerance. The measured resistivity was estimated to be about $1.2x10^{14}$ Ω.cm and dark current density ranges between pA/cm^2 to a fraction of few nA/cm^2.

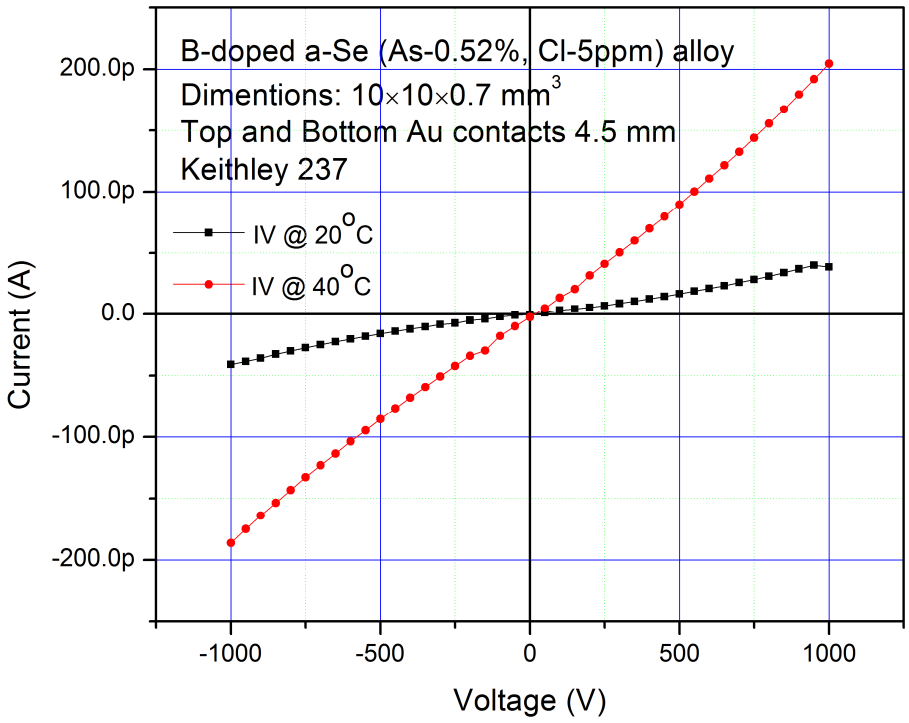

Figure 4.7. Current (I)-voltage (V) characteristics of boron doped a-Se alloy at 20°C and 40°C.

Table 4.2. Resistivity of characterized B-doped a-Se alloy.

B-doped a-Se(As-0.52%, Cl-5ppm) alloy	Voltage range (V)	Current range (pA)	Mean Resistance (Ω)	Resistivity (Ω-cm)
@40°C	Min=-1000 Max=1000	Min=-186.3 Max=204.7	5.38×10^{12}	1.53×10^{13}
@20°C	Min=-1000 Max=1000	Min=-40.9 Max=38.6	2.67×10^{13}	1.17×10^{14}

4.8 CONCLUSIONS

Boron doped a-Se (As, Cl) alloys were synthesized with various natural isotropic boron (^{10}B) concentrations. The compositions of the synthesized alloys were characterized by ICP/MS analysis. The characterization results show that the synthesized alloys are amorphous in nature, have good surface properties and free from parasitic defects. The XPS survey scans correspond very well with a-Se (B, As, Cl) alloying elements, show an uniform distribution of the elements, and confirm the absence of any compound (e.g., B_2Se_3 or B_2SeO_4) formations. The devices fabricated based on B-doped a-Se (As, Cl) alloy were photosensitive at 400nm and were highly resistive with very low level of leakage current.

CHAPTER 5: DETECTOR TESTING TO DEMONSTRATE THERMAL NEUTRON DETECTION CAPABILITIES

5.1 BACKGROUND

As discussed in chapter 1, we know that semiconductors need certain properties to function as radiation detectors. Amorphous selenium alloyed with arsenic and chlorine has the required material qualities to function as a good photoconductor and x-ray detector for imaging applications. However its use as a radiation detector for thermal neutron detection is not widely developed and understood. Although radiation detection depends on the optical, electrical and material properties of the semiconductor, it is important to understand the signal processing techniques and electrical engineering involved to device a suitable detection scheme.

Therefore, to demonstrate the feasibility of ^{10}B-doped a-Se (As 0.52%, Cl 5ppm) as thermal neutron detector, the final and most important characterization is to evaluate detector response to the charged radiation particles. As explained in Section 1.7, the use of boron-doped a-Se (As, Cl) film as an efficient thermal neutron detector relies on the presence of ^{10}B, which has a large cross section for thermal neutrons (3840 barns), and the neutrons when captured by the ^{10}B nucleus undergo an reaction, producing charged alpha (α) particles. Consequently, if we can monitor the alpha particle response, we can indirectly account for neutrons. In our investigation, ^{241}Am α-particle source was thus used to evaluate the response of the fabricated detectors.

5.2 EXPERIMENTS WITH ALPHA PARTICLES

For detector testing, alpha (α) particles were employed as a surrogate for neutrons because of the comparative radiological ease of use of small alpha sources (^{241}Am) and the fact that ^{10}B neutron capture reaction directly produces an alpha particle. The standard nuclear instrumentation used were preamplifier, shaping amplifier and multi-channel analyzers (MCA) as shown schematically in Figure 5.1. The detector device is mounted on an insulating alumina plate, onto a stud inside an EMI shielded aluminum box. Figure 5.2 shows a picture of the test set up for alpha exposure.

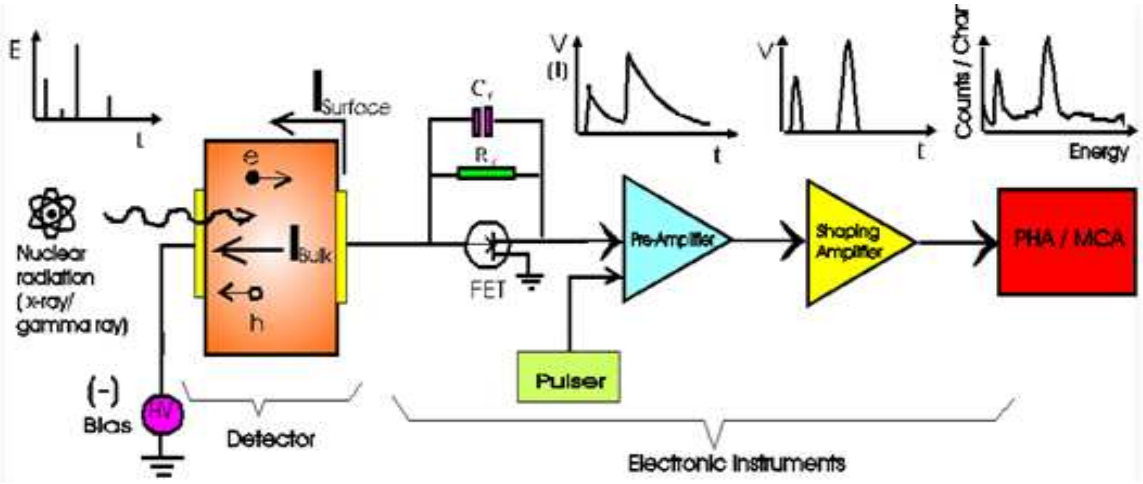

Figure 5.1. Schematics of the experimental setup used for ^{241}Am alpha signal detection.

The semitransparent negatively biased front gold (Au) contact of the B-doped a-Se (As, Cl) planner detector device (described in Section 4.7) was exposed to alpha particles. The front contact is biased at -1000 volts. When this charged particle interacts with the detector it ionizes and under a DC bias electron and holes pairs are collected by the detector's electronics. This collected charge is then converted to a corresponding voltage which is subsequently processed by charge sensitive preamplifier, connected to

the front and back contacts. The output of the charge sensitive preamplifier is connected to a spectroscopy amplifier. During the exposure and extraction of data the system is constantly evacuated, using a rotary pump, in order to minimize scattering of alpha-particle with air molecules.

The pulses emerging from the spectroscopy amplifier are then recorded with a multi-channel pulse-height analyzer. This information is recorded in the form of a pulse height spectrum which gives the counts of radioactive interactions for corresponding energy values.

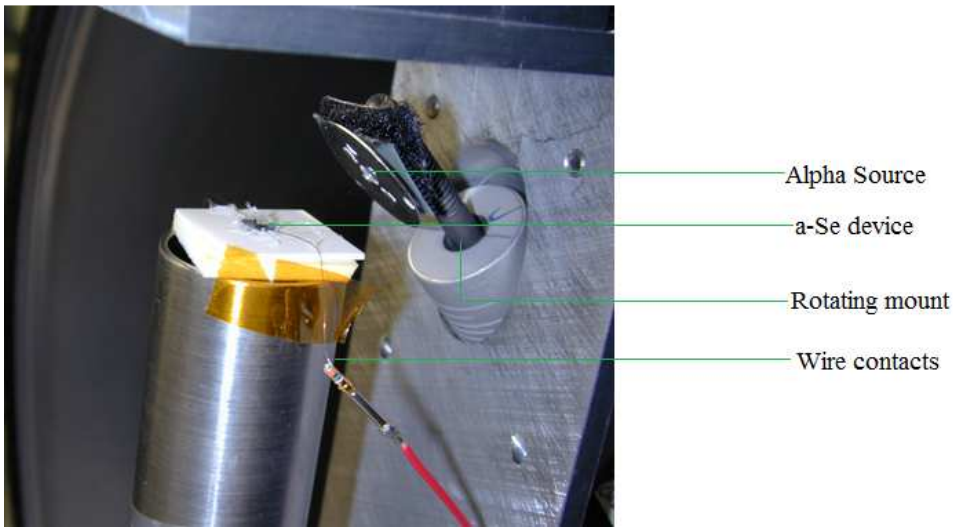

Figure 5.2. A picture of alpha exposure setup.

5.3 RESULTS

Figure 5.3 Figure 5.2. A picture of alpha exposure setup.shows the pulse-height spectrum obtained by irradiating B-doped a-Se (As, Cl) alloy detector with source and. Thickness of the alloy film was ~320 micron and the top contact area exposed to the source was 5 mm^2. The spectrum was acquired at room temperature (295K) and in

vacuum as explained above. This spectrum completely vanishes when a piece A4 white copying paper was placed in between the radiation source and detector confirming the detector's response to alpha particles.

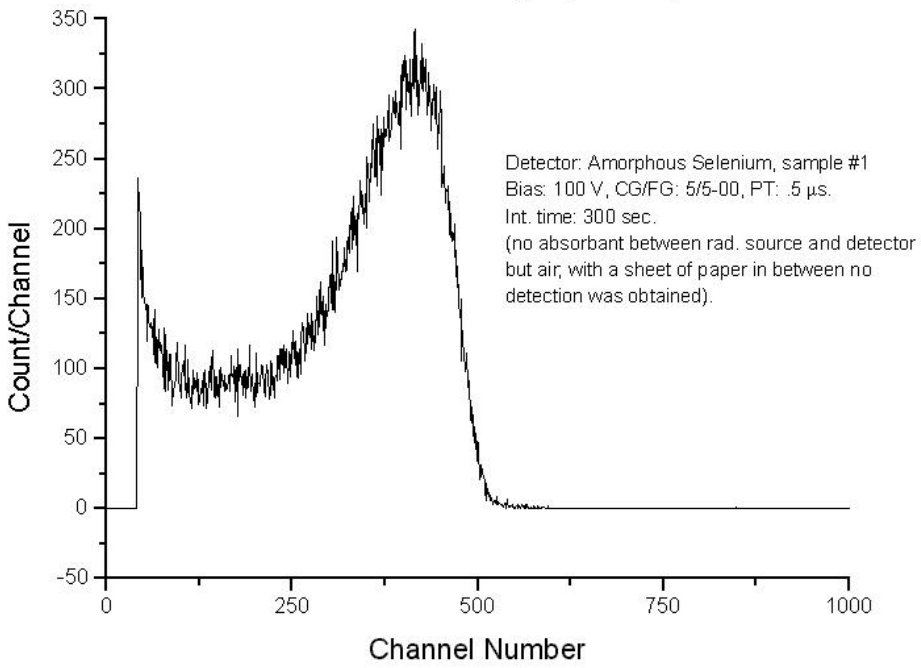

Figure 5.3. Pulse Height Spectrum obtained by irradiating B-doped a-Se (As, Cl) alloy film detector with ^{241}Am source.

Alpha spectrum in Figure 5.3 shows fairly broad peak with increase in count rate in low channels. The source ^{241}Am used is not mono-energetic. The main alpha energies are 5485.7 keV (86%) and 5443.0 keV (13%). The measured energy and energy resolution are both influenced by the source-detector geometry. Even though the resolution should be improved, the spectrum clearly demonstrates that B doped a-Se (As, Cl) alloy detector is capable of spectroscopic performance at room temperature for high-energy photons of alpha particles.

CHAPTER 6: CONCLUSION AND FUTURE WORKS

6.1 CONCLUSION

The goal of the research effort was to synthesize B-doped a-Se (As, Cl) alloy material, characterize and demonstrate the feasibility of this material as a solid-state semiconductor for high energy particle detectors such as neutron.

To achieve this goal, first, Se precursor material was purified by zone refining technique and was used to make Se-As and Se-Cl master alloys. These master alloys were used to synthesize a-Se (As, Cl) bulk alloys, and subsequently B-doped a-Se (As, Cl) alloys. A specially designed palletizing alloying reactor was used to synthesize these aforementioned alloys. The compositions of the synthesized alloys were confirmed by ICP/MS analysis.

The alloys were thoroughly characterized to understand their optical, electrical, and spectroscopic properties. The characterization results showed that the synthesized alloys were amorphous in nature and were free from parasitic defects. Furthermore, experimentally determined physical properties like melting point, crystallization temperature, bandgap energy, etc. were in agreement with what is found in the literature. The XPS survey scans correspond very well with a-Se (B, As, Cl) alloying elements, show an uniform distribution of the elements, and confirm the absence of any compound (e.g., B_2Se_3 or B_2SeO_4) formations. The devices fabricated based on B-doped a-Se (As,

Cl) alloy were photosensitive at 400 nm and were highly resistive with very low level of leakage current.

We were successful in the synthesis of B-doped (up to 18 a/o) a-Se (As, Cl) alloy in large quantities and were able to make 1″ x 1″films on ITO and oxidized aluminum substrates up to a thickness of 320 μm. With these films, planar detectors have been fabricated and characterized. Detector testing has been conducted at room temperature using ^{241}Am α-source. The pulse-height spectrum clearly demonstrates that B-doped a-Se (As, Cl) alloy detector is capable of detecting high-energy alpha particles which was used as the surrogate of thermal neutrons.

6.2 FUTURE WORKS

While B-doped a-Se (As, Cl) alloy based detector successfully demonstrated its capability as thermal neutron detector at room temperature, there are several areas for further investigation in order to increase the spectroscopic resolution of these detectors. Some of the recommended investigations for future studies are:

- Investigations of different doping effects to obtain optimum device performance. Higher boron doping is expected to generate higher signals for neutrons, but there can be other effects due to very high concentration of dopants or heavy doping effects and mechanical properties [53].
- Determination of electron-hole pair creation energy and charge-transport property ($\mu\tau$ product) by quantitative evaluation of trapping lifetime (τ) and the mobility (μ) which will be useful to optimize the detector performances [12, 54, 55].
- Investigation of junction properties between B-doped a-Se (As, Cl) alloys and a variety of metal contacts with different work functions to determine whether the

choice of metal can improve the signal-to-noise ratio of neutron detectors. [56, 14]

- Because hole mobility of a-Se is about 20 times higher than that of electrons, further improvement can be achieved by using advanced electrode geometry instead of planar electrodes such as Frisch ring, coplanar grid structure, and pixilated structures, which have been reported to improve resolution of devices significantly in CdZnTe radiation detectors. [57, 58, 59, 13, 60]

REFERENCES

[1] S. M. Gruner, "X-ray imaging detectors," *Phys. Today* , vol. 65, no. 12, pp. 29-34, 2012.

[2] J. Yorkston, "Recent developments in digital radiography detectors," *Nucl. Inst. Meth. A*, vol. 580, no. 2, pp. 974-985, 2007.

[3] S. Kasap, J. B. Frey, G. Belev, O. Tousignant, H. Mani, J. Greenspan, L. Laperriere, O. Bubon, A. Reznik, G. DeCrescenzo, K. S. Karim and J. A. Rowlands, "Amorphous and Polycrystalline Photoconductors for Direct Conversion Flat Panel X-Ray Image Sensors," *Sensors*, vol. 11, pp. 5112-5157, 2011.

[4] H. K. Kim, C. H. Lim, J. Tanguay, S. Yun and I. A. Cunningham, "Spectral analysis of fundamental signal and noise performances in photoconductors for mammography," *Med Phys.*, vol. 39, no. 5, pp. 2478-90, 2012.

[5] P. Bennett, K. Shah, L. Cirignano and M. Klugerman, "Characterization of polycrystalline TlBr films for radiographic detectors," *IEEE Transactions on Nuclear Science*, vol. 46, no. 3, pp. 266-270, 1999.

[6] Y. Kang, L. E. Antonuk and a. L. H. Y. El-Mohri, "Examination of PbI_2 and HgI_2 photoconductive materials for direct detection, active matrix, flat-panel imagers for diagnostic X-ray imaging," *IEEE Transactions on Nuclear Science* , vol. 52, no. 1, pp. 38-45, 2005.

[7] R. A. Street, S. E. Ready, K. V. Schuylenbergh, J. Ho, J. B. Boyce, P. Nylen, K. Shah, L. Melekhov and H. Hermon, "Comparison of PbI_2 and HgI_2 for direct detection active matrix x-ray image sensors," *J. Applied Physics*, vol. 91, no. 5, pp. 3345-3355, 2002.

[8] A. Owens and A. Peacock, "Compound semiconductor radiation detectors," *Nuclear Instruments and Methods in Physics Research A*, vol. 531, pp. 18-37, 2004.

[9] M. Z. Kabir and S. O. Kasap, "Charge collection and absorption-limited sensitivity of x-ray photoconductors: Applications to a-Se and HgI_2," *Appl. Phys. Lett.*, vol. 80, p. 1664, 2002.

[10] S. D. Sordo, L. Abbene, E. Caroli, A. M. Mancini, A. Zappetteni and P. Ubertini, "Progress in the Development of CdTe and CdZnTe Semiconductor Radiation Detectors for Astrophysical and Medical Applications," *Sensors*, vol. 9, pp. 3491-3526, 2009.

[11] T. Schlesinger, J. Toney, H. Yoon, E. Lee, B. Brunett, L. Franks and R. James, "Cadmium zinc telluride and its use as a nuclear radiation detector material," *Materials Science and Engineering*, vol. 32, pp. 103-189, 2001.

[12] S. K. Chaudhuri, K. J. Zavalla, R. M. Krishna and K. C. Mandal, "Biparametric analyses of charge trapping in $Cd_{0.9}Zn_{0.1}Te$ based virtual Frisch grid detectors," *J. Appl. Phys.*, vol. 113, pp. 074504-1-6, 2013.

[13] R. M. Krishna, S. K. Chaudhuri, K. J. Zavalla and K. C. Mandal, "Characterization of $Cd_{0.9}Zn_{0.1}Te$ based virtual Frisch grid detectors for high energy gamma ray detection," *Nuclear Instruments and Methods in Physics Research A*, vol. 701, pp. 208-213, 2013.

[14] K. C. Mandal, R. M. Krishna, P. G. Muzykov and T. C. Hayes, "Fabrication and characterization of high barrier $Cd_{0.9}Zn_{0.1}Te$ Schottky Diodes for high resolution nuclear radiation detectors," *IEEE Transactions on Nuclear Science*, vol. 59, pp. 1504 - 1509, 2012.

[15] Z. Ji, L. Li and J. Xi, "Deposition of PbO thin films and its X-ray photoconductive properties," in *International Conference on Multimedia Technology (ICMT)*, 2011.

[16] M. Simon, S. Grabowski, B. Menser, G. Much, A. Nascetti, M. Overdick, D. Wiechert, R. Ford, A. Franklin and M. Powell, "Analysis of lead oxide (PbO) layers for direct conversion X-ray detection," in *IEEE proceeding of Nuclear Science Symposium Conference*, Issue 7, 2004.

[17] S. Kasap, J. B. Frey, G. Belev, O. Tousignant, H. Mani, L. Laperriere, A. Reznik and J. A. Rowlands, "Amorphous selenium and its alloys from early xeroradiography to high resolution X-ray image detectors and ultrasensitive imaging tubes," *Phys. Status Solidi B*, vol. 246, no. 8, pp. 1794-1805, 2009.

[18] R. Zallen and G. Lucovsky, In Selenium (R. A. Zingaro and W.C. Cooper, eds.), New York: Van Nostrand, 1974.

[19] J. Mort, "Xerography: A study in innovation and economic competitiveness," *Physics Today*, vol. 32, no. April, 1994.

[20] I. Blevis, D. Hunt and J. Rolands, "Measurement of x-ray photogeneration in amorphous selenium," *J. Appl. Phys*, vol. 85, p. 7958, 1999.

[21] S. O. Kasap and J. A. Rowlands, "Review: X-ray photoconductors and stabilized a-Se for direct conversion digital flat-panel X-ray imagedetectors," *Journal of materials science: materials in electronics*, vol. 11, pp. 179-198, 2000.

[22] E. Fourkal, M. Lachaine and B. G. Fallone, "Signal formation in amorphous-Se-based x-ray detectors," *Phys. Rev. B*, vol. 63, p. 195204, 2001.

[23] D. Moses, "Mechanism of carrier photogeneration in amorphous selenium: Fast transient photoconductivity," *Phys. Rev. B*, vol. 53, no. 8, p. 4462, 1996.

[24] M. Hoheisel and L. Batz, "Requirements on amorphous semiconductors for medical X-ray detectors," *Journal of Non-Crystalline Solids*, Vols. 266-269, pp. 1152-1157, 2000.

[25] O. Bubon, G. DeCrescenzo, J. A. Rowlands and A. Reznik, "Amorphous selenium (a-Se) avalanche photosensor with metal electrodes," *Journal of Non-Crystalline Solids*, vol. 358, p. 2431–2433, 2012.

[26] S. Kasap, C. Haugen, M. Nesdoly and J. Rowlands, "Properties of a-Se for use in flat panel X-ray image detectors," *J. Non-Crystalline Solids*, vol. 1163, pp. 266-269, 2000.

[27] P. Jo´va´ri, R. G. Delaplane and L. Pusztai, "Structural models of amorphous selenium," *Phys. Rev. B,* vol. 67, p. 172201, 2003.

[28] Y. Wang and C. H. Champness, "Xerographic effects of small chlorine additions to amorphous selenium," *J. Appl. Phys.,* vol. 77, p. 722, 1995.

[29] C. Allen, G. Belev, R. Johanson and S. Kasap, "Relaxation of the electrical properties of vacuum-deposited a-$Se_{1-x}As_x$ photoconductive films: Charge-carrier lifetimes and drift mobilities," *J. Vac. Sci. Technol. A,* vol. 28, p. 1145, 2010.

[30] S. Kasap, K. Koughia, B. Fogal, G. Belev and R. Johanson, "The influence of deposition conditions and alloying on the electronic properties of amorphous selenium," *Fizika i Tekhnika Poluprovodnikov,* vol. 37, no. 7, pp. 816-821, 2003.

[31] V. Radeka, N. A. Schaknowski, G. C. Smith and B. Yu, "High Performance Imaging Neutron Detectors," *Nucl. Instrum. & Meth.,* vol. A419, pp. 642-647, 1998.

[32] G. Knoll, Radiation Detection And Measurement, 3d ed., New York: John Wiley and Sons, 1999.

[33] A. Allen, P. Schofield and D. Ross, Position Sensitive Detection of Thermal Neutrons, London: Academic Press, 1983.

[34] W. Feller, R. Downing and P. White, "Neutron field imaging with microchannel plates," *Proc. SPIE,* vol. 4141, p. 291, 2000.

[35] J. Chaput, M. Caria, F. Laverroux, B. Surre and J. Maublant, "Results on a prototype of a large-area X-ray imaging device using CMOS hybrid detectors," *Nucl. Instr. Methods in Phys. Res. A,* vol. 555, p. 236, 2005.

[36] W. G. Pfann, Zone Melting, Florida: Krieger Publishing, 1978.

[37] S. O. Kasap, The Handbook of Imaging Materials, 2nd ed., New York: Marcel Dekker, 1998.

[38] A. Date and A. Gray, Applications of Inductively Coupled Plasma Source Mass Spectrometry, Glasgow: Blackie, 1989.

[39] A. K. Bandyopadhyay, "Pressure-induced phase transformations in amorphous selenium by x-ray diffraction and Raman spectroscopy," *Phys. Rev. B,* vol. 54, no. 17, p. 12 049, 1996.

[40] L. Reimer, Scanning electron microscopy : physics of image formation and microanalysis, New York: Springer, 1998.

[41] G. Lucovsky, A. Mooradian, W. Taylor, J. Wright and R. C. Keezer, "Identification of the fundamental vibrational modes of trigonal, α - monoclinic and amorphous selenium," *Solid State Commun,* vol. 5, p. 113, 1967.

[42] M. Gorman and S. Solin, "Transmission Raman and depolarization spectra of bulk a-Se from 13 to 300 cm^{-1}," *Solid State Commun,* vol. 18, p. 1401, 1976.

[43] V. V. Poborchii, A. V. Kolobov and K. Tanaka, "An in situ Raman study of polarization-dependent photocrystallization in amorphous selenium films," *Appl. Phys. Lett.,* vol. 72, p. 1167, 1998.

[44] I. L. Li, S. C. Ruan, Z. M. Li, J. P. Zhai and Z. K. Tang, "Resonant Raman study of confined Se single helix and Se8 rings," *Appl. Phys. Lett.,* vol. 87, p. 071902, 2005.

[45] V. S. Minaev, S. P. Timoshenkova and V. V. Kalugina, "Structural and phase transformation in condensed selenium," *Journal of Optoelectronics and Advanced Materials,* vol. 7, no. 4, pp. 1717-1741, 2005.

[46] A. H. Pinto, E. R. Leite, E. Longo and E. R. d. Camargo, "Crystallization at room temperature from amorphous to trigonal selenium as a by product of the synthesis of water dispersible zinc selenide," *Materials Letters,* vol. 87, pp. 62-65, 2012.

[47] S. N. Yannopoulos and K. S. Andrikopoulos, "Raman scattering study on structural and dynamical features of noncrystalline selenium," *J. Chem. Phys.,* vol. 121, p. 4747, 2004.

[48] J. Holubová, Z. Cˇernošek and E. Cˇernošková, "The selenium based chalcogenide glasses with low content of As and Sb: DSC, StepScan DSC and Raman spectroscopy study," *Journal of Non-Crystalline Solids,* vol. 355, pp. 2050-2053, 2009.

[49] G. W. H. Höhne, W. F. Hemminger and H.-J. Flammersheim, Differential Scanning Calorimetry, 2nd Ed, New York: Springer, 2003.

[50] N. Mott and D. E.A., Electronic Processes in Non-crystalline Materials, Oxford: Clarendon Press, 1979.

[51] K. Okano, I. Saito, T. Mine, Y. Suzuki, T. Yamada, N. Rupesinghe, G. Amaratunga, W. Milne and D. Zahn, "Characterizations of a-Se based photodetectors using X-ray photoelectron spectroscopy and Raman spectroscopy," *Journal of Non-Crystalline Solids,* vol. 353, no. 3, pp. 308-312, 2007.

[52] S. Abbaszadeh, N. Allec, S. Ghanbarzadeh, U. Shafique and K. S. Karim, "Investigation of Hole-Blocking Contacts for High-Conversion-Gain Amorphous Selenium Detectors for X-Ray Imaging," *IEEE Trans. on Electron Devices,* vol. 59, no. 9, p. 2403, 2012.

[53] Z. Rak, S. Mahanti, K. C. Mandal and N. Fernelius, "Doping dependence of electronic and mechanical properties of $GaSe_{1-x}Te_x$ and $Ga_{1-x}In_xSe$ from first principles," *Phys. Rev. B,* vol. 82, pp. 155203-1-10, 2010.

[54] S. K. Chaudhuri, K. M. Zavalla and K. C. Mandal, "Experimental Determination of Electron-Hole Pair Creation Energy in 4H-SiC Epitaxial Layer: An Absolute Calibration Approach," *Appl. Phys. Lett.,* vol. 102, p. 031109, 2013.

[55] K. C. Mandal, R. M. Krishna, P. G. Muzykov, S. Das and T. S. Sudarshan, "Characterization of Semi-Insulating 4H Silicon Carbide for Radiation Detectors," *IEEE Transactions on Nuclear Science,* vol. 58, pp. 1992-1999, 2011.

[56] S. H. Majid and R. E. Johanson, "Studies on excess noise in stabilized amorphous selenium used in X-ray photodetectors," *Journal of Non-Crystalline Solids,* vol. 354, pp. 2763-2766, 2008.

[57] W. J. McNeil, D. S. McGregor, A. E. Bolotnikov, G. W. Wright and R. B. James, "Single-charge-carrier-type sensing with an insulated Frisch ring CdZnTe semiconductor radiation detector," *Appl. Phys. Lett.,* vol. 84, p. 1988, 2004.

[58] P. N. Luke, "Single-polarity charge sensing in ionization detectors using coplanar electrodes," *Appl. Phys. Lett,* vol. 65, p. 2884, 1994.

[59] A. E. Bolotnikov, W. R. Cook, S. E. Boggs, F. A. Harrison and S. M. Schindler, *Nucl. Instrum. Methods Phys. Res. A*, vol. 458, p. 585, 2001.

[60] K. C. Mandal, S. H. Kang, M. Choi, A. Kargar, M. J. Harrison, D. S. McGregor, A. Bolotnikov, G. Carin, G. Camarda and R. James, "Characterization of Low-Defect $Cd_{0.9}Zn_{0.1}Te$ and CdTe Crystals for High-Performance Frisch Collar Detector," *IEEE Transactions on Nuclear Science*, vol. 54, no. 4, pp. 802-806, 2007.